Seismic Wave Propagation and Earth models

Peter Bormann[1], E. Robert Engdahl[2], and Rainer Kind[1]

[1] Formerly GFZ German Research Center for Geosciences, Department 2: Physics of the Earth, Telegrafenberg, 14473 Potsdam, Germany; E-mail: pb65@gmx.net and kind@gfz-potsdam.de;

[2] University of Colorado, Department of Physics, Boulder, CO 80309, USA; E-mail: Bob.Engdahlt@Colorado.EDU

2.6 Seismic phases and travel times in real Earth (P. Bormann)

Seismic body waves propagate three-dimensionally and are more strongly affected than surface waves by refraction, reflection and mode conversion at the main impedance contrasts in the radial direction of the Earth. This gives rise, with growing distance, to the appearance of more and more secondary seismic body-wave phases following the direct P- and S-wave arrivals in seismic records (e.g. Fig. 2.25). And since body waves show no dispersion in the considered frequency range these phases can usually be well observed and discriminated from each other as long as their travel-time curves do not overlap.

All of these secondary phases have a special story to tell about the geometrical and physical properties of the discontinuities which they encountered during their travel through the Earth's interior and which have shaped their waveforms and influenced their amplitude and frequency content. Therefore, the proper identification and parameter or waveform reporting about later phases in seismic records to relevant data centers is an important duty of seismological observatories. In addition, the complementary use of secondary phases significantly improves the precision and accuracy of seismic event locations, their source depth in particular (see Figure 7 in IS 11.1 and section 2.6.3). In the following, we will introduce the main types of seismic body-wave phases that can generally be observed at local, regional and teleseismic distance ranges. They should be identified, analyzed and reported by

seismic observatories or data analysis centers. Basic features of their travel-time curves, polarization, waveforms and frequency range of observation, which can guide their identification, will be presented.

2.6.1 Seismic phases and travel times from local and regional events

Seismic waves arriving at stations at local distances of up to about 150 km or regional distances of up to about 15° (1° = 111.2 km) from the seismic source have traveled exclusively or dominatingly through the crust or the sub-crustal uppermost mantle. The crust varies strongly in its thickness (see Fig. 2.11), petrologic composition and internal structure due to folding and faulting processes in the past. The resulting strong heterogeneities in physical properties at scale length of several decameters to several km cause intensive scattering of P and S waves in the typical frequency range for the recording of near seismic events (about 0.5 to 50 Hz). Therefore, primary wave onsets are usually followed by signal-generated noise or coda waves that make it difficult to identify later seismic phases reflected or refracted from weaker intra-crustal discontinuities. It is usually only the significant velocity increase of about 20% at the base of the crust towards the upper mantle (*Mohorovičić discontinuity*, or *Moho* for short), which produces first or later wave onsets besides the direct P and S waves that are strong enough to be recognizable above the ambient or signal-generated noise level. Only in some continental regions may an intermediate discontinuity, named the *Conrad discontinuity* after its discoverer, produce recognizable critically refracted (Pb = P*; Sg = S*) or reflected waves (see Fig. 2.46). Accordingly, for purposes of routine seismological observatory practice, it is usually sufficient to represent the crust as a horizontal one-layer model above the half-space (upper mantle).

Both of the widely used global 1-D Earth velocity models, IASP91 by Kennett and Engdahl (1991) and AK135 by Kennett et al. (1995) assume a homogeneous 35 km thick two-layer crust with the intermediate crustal discontinuity at 20 km depth (see DS 2.1). The respective average velocities for the upper and lower crust and the upper mantle are for P waves 5.8 km/s, 6.5 km/s and 8.04 km/s, and for S waves 3.36 km/s, 3.75 km/s and 4.47 km/s, respectively. The *impedance contrast* at the Conrad discontinuity and the Moho is about 1.3. Fig. 2.46 is a simplified depiction of such a two-layer crust and of the seismic rays of the main crustal/upper mantle phases to be expected. These are: Pg, Sg, Pb, Sb, Pn, Sn, PmP and SmS. For detailed definition of the phase names see IS 2.1 or Storchak et al. (2003 and 2011).
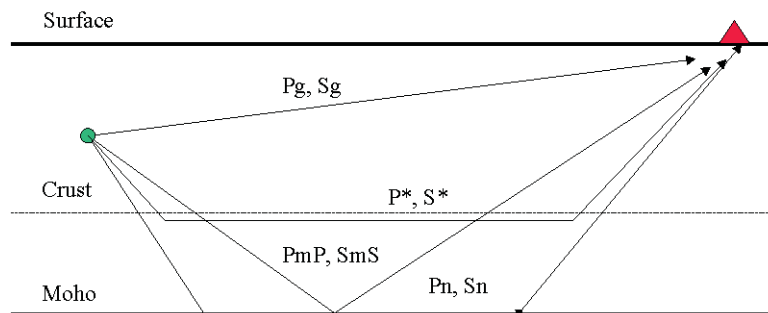

Fig. 2.46 A simplified model of the crust showing the ray traces of the main "crustal phases" observed for near (local and regional) earthquakes. Note: P* = Pb and S* = Sg.

The apparent horizontal velocity of the reflected PmP and SmS waves varies with distance according to their changing incidence angle on the surface. Their travel-time branches form hyperbolae that approach asymptotically the travel-time curves for Pg and Sg (or Pb and Sb) with increasing distance (see Fig. 2.47). Note that Pn, if a head wave, has usually smaller amplitudes than Pg and Sg, at least for distances up to about 300 km. Pn can be usually identified above the noise level only when it becomes the P-wave first arrival. At larger distances, because of the stronger attenuation of upper crustal Pg and Sg and with Pn and Sn being less attenuated as typically upper mantle diving phases, Pn and Sn may become clear P and S first arrivals (see Fig. 2.17). Beyond the critical point (at about 70-80 km distance for an average crust) the super-critically reflected waves PmP and SmS have generally the largest amplitudes, however, arriving always closely after Pg and Sg, their onset times can usually not be picked reliably enough as to be of value for earthquake location. Therefore, these phases are usually not explicitly reported in routine observatory practice. However, reporting of Pg, Sg, Pn and Sn, if recognizable, is a must. This also applies to the reporting of the maximum amplitudes in records of near seismic events for the determination of local magnitudes Ml (see Chapter 3, section 3.2.4). Depending on source depth too, this amplitude maximum may be related to Sg/SmS, Lg, or Rg (see Figs. 2.17, 2.18 and 2.47). A simple average local travel-time curve for a single-layer crust in Central Europe had been derived from related reliable phase observations at European observatories from an earthquake in Hungary decades ago. It is depicted in Fig. 2.48 and proved to be a suitable single-layer crust approximation for routine analysis, phase identification and location of seismic events in the considered area (see EX 11.1). The crustal und sub-Moho velocity data given in DS 2.1 for IASP91 and AK 135, respectively, would permit to calculate a similar global average travel-time curve.
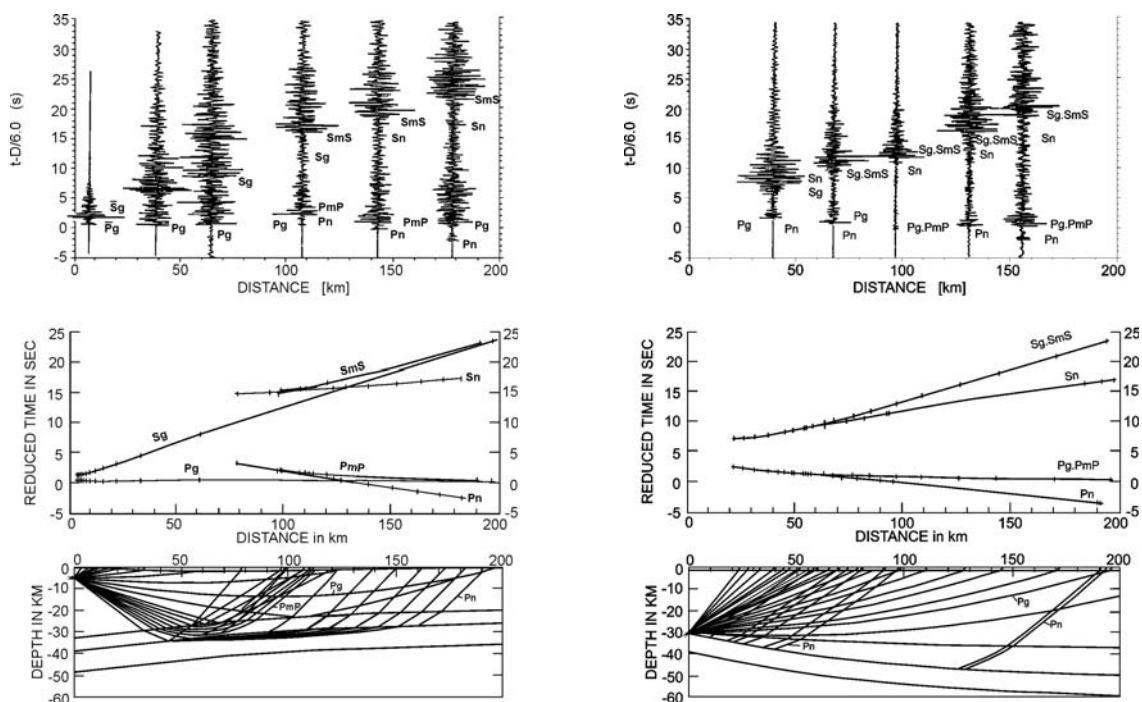

Fig. 2.47 Records (above) of two regional earthquakes of Oct. 9, 1986 at Sierre (left) and of July 7, 1985 at Langenthal, Switzerland together with the calculated reduced travel-time curves (middle) and ray-tracing crustal models which best fit the observations (below), redrawn and complemented from Kulhánek (1990), Anatomy of Seismograms, plate 4, pp. 83-84, © (with permission from Elsevier Science).
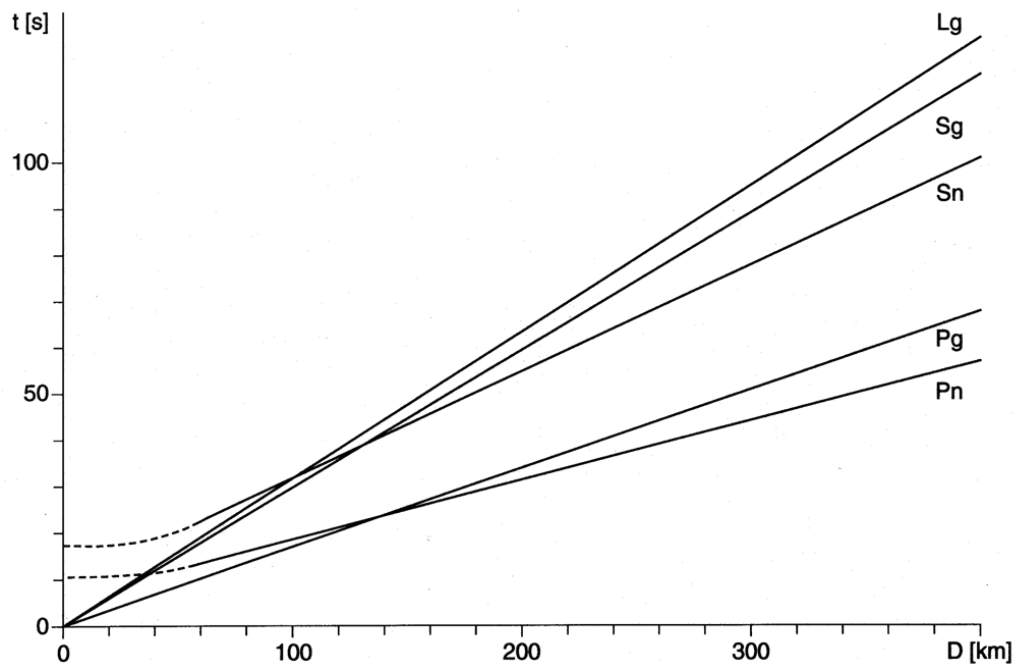
Fig. 2.48 Empirically determined average travel-time curves for the phases Pn, Pg, Sn, Sg and Lg observed at distances up to 400 km, assuming a single-layer crust in Central Europe.

However, crustal travel-time curves based on a global velocity model may not be representative at all for certain regions and may serve as a starting model only to work with. It is one of the main tasks of operators of local and regional seismic networks to derive from their own carefully analyzed data of near events not only local/regional magnitude calibration functions (see 3.2.4.3 and Table 2 in DS 3.1) but also average local/regional 1-D travel-time curves. The latter will not only allow significantly improved seismic event locations but may serve also as starting models for tomographic studies of crustal heterogeneities and the derivation of 3-D velocity models.

Fig. 2.47 above shows real short-period seismic network records of two local earthquakes in Switzerland in the distance range between about 10 km and 180 km along different profiles together with the modeling of their reduced travel-time curves and inferred structural profiles. While one event was at a depth of only 5 km, the other event was about 30 km deep. The first one was observed by stations situated up-dip while the latter event was observed down-dip. The striking differences in the shape and gradient of the travel-time curves and in the crossover distance between Pg and Pn, in particular, are obvious. In the case of the deeper event near to the Moho, Pn becomes the first arrival beyond 70 km distance, whereas for the shallower event Pn outruns Pg only at more than 130 km epicenter distance. In both cases Pg (Sg) and/or PmP (SmS) are the prominent P and S arrivals. The Pn first arrivals are relatively small. No Pb, Sb or reflected waves from a mid-crustal discontinuity are recognizable in Fig. 2.47. Note, however, depending on the orientation of the earthquake rupture and thus of the related radiation characteristic of the source, it may happen that a maximum of energy is radiated in the direction of the Pn ray and a minimum in the direction of the Pg ray. Then the usual relationship $A_{Pn} < A_{Pg}$ may be reversed (examples are given in Chapter 11, section 11.5.1).

Misinterpretation of Pn as Pg or vice versa may result in large errors of event location. Therefore, one should have at least a rough idea at which distance in the region under study, depending on the average crustal thickness and velocity, one may expect Pn to become the first arrival. A "rule-of-thumb" for calculating the crossover distance x_{co} is given in Eq. (6) of IS 11.1. For an average single-layer crust and a surface source, $\mathbf{x_{co} \approx 5\ z_m}$ with z_m – Moho depth. However, as demonstrated with Fig. 2.47, x_{co} is only about half as large for near Moho earthquakes and also the dip of the Moho and the direction of observation (up- or downdip) do play a role. Yet, lower crustal earthquakes are rare in a continental (intraplate) environment. Mostly they occur in the upper crust. Rules-of-thumb for calculating the source distance from the travel-time differences Sg-Pg and Sn-Pn are:

hypocenter distance d [in km] $\approx \Delta t(\mathrm{Sg\text{-}Pg})$ [in s] $\times 8$ (near range only)   (2.35)

epicenter distance D [in km] $\approx \Delta t(\mathrm{Sn\text{-}Pn})$ [in s] $\times 10$ (in Pn-Sn range < 15°)   (2.36)

Sometimes, very strong onsets after Pg, well before Sn or Sg are observed and may complicate proper interpretation of local phases on the basis of an oversimplified travel-time model as the one in Fig. 2.48. Then special modelling may be required, which is beyond the scope of seismic routine analysis. According to Bock et al. (1996) these strong onsets (**?**) may be related to local depth phases (e.g., sPmP in Fig. 2.49).
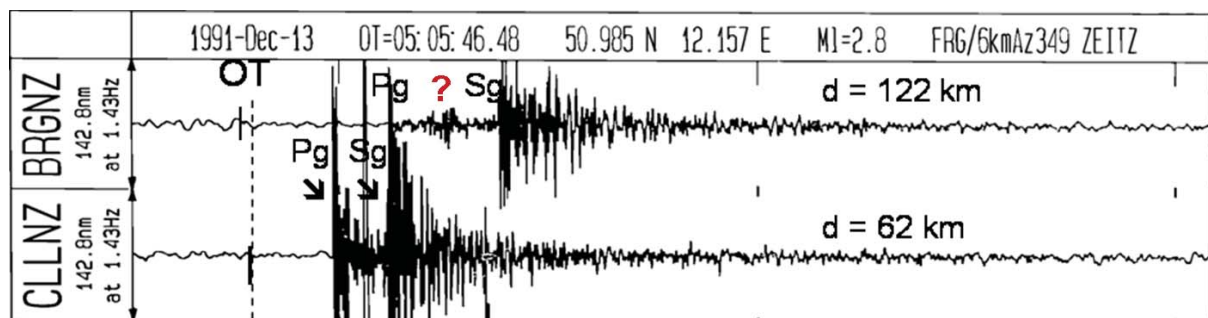

Fig. 2.49 Two records of a local earthquake at a source depth of h = 6 km in eastern Germany. The strong seismic phase **?** between the onsets of Pg and Sg at hypocenter distance of 122 km in the record of station BRG can not be identified by using the simplified set of travel-time curves for surface foci in Fig. 2.48. According to model calculations it is most likely the depth phase sPmP of the large amplitude overcritical reflection PmP from the Moho discontinuity.

Also be aware that in the case of sub-crustal earthquakes, which are common in subduction zones, none of the crustal phases discussed above exist. In this case, the first arriving longitudinal and shear wave onsets are usually termed P and S, respectively, as for teleseismic events (see Fig. 2.50) although the IASPEI standard phase nomenclature terms them also Pn and Sn for upgoing rays from the source that are recorded in the local distance (see Figure 1c in IS 2.1; Storchak et al. 2003 and 2011).
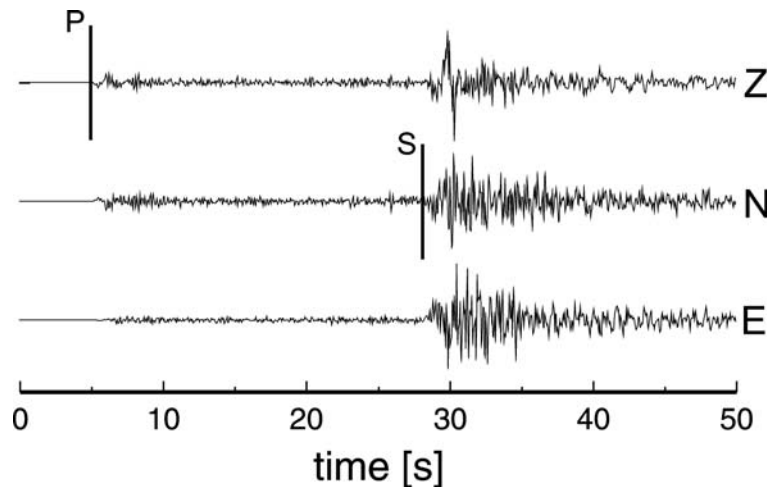
Fig. 2.50 P- and S-wave onsets from a local earthquake in northern Chile at a depth of 110 km and a hypocenter distance of about 240 km (courtesy of B. Schnurr, 2001).

2.6.2 Shallow source body-waves and travel times at teleseismic distances

Seismic waves arriving at distances beyond 10° up to about 30° have mainly traveled through the upper mantle (from Moho to about 410 km depth) and the transition zone to the lower mantle (between about 410 km and 660 km depth). The strong discontinuities which mark the upper and lower boundary of the transition zone are associated with strong increases in seismic impedance (i.e., of both velocity and density; see Fig. 2.7). This results in two remarkable triplications of the travel-time curve for P waves (see Fig. 2.32) and S waves, which give rise to complicated waveforms of rather long duration (about 10 s and more) and consisting of a sequence of successive onsets with different amplitudes (Fig. 2.51).
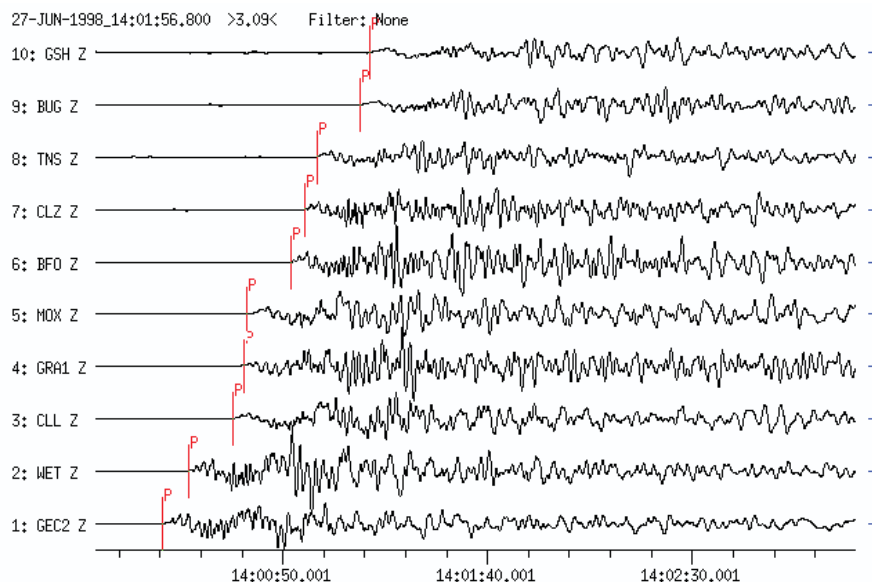

Fig. 2.51 Broadband seismograms with high time resolution showing the complex P-wave groups in records of an earthquake in southern Turkey at stations of the German Regional Seismograph Network (GRSN) at epicenter distances between D = 19.7° (GEC2) and 24.8° (GSH).

For epicenter distances D > 30° P and S waves are followed by an increasing number of secondary waves, mainly phases, which have been reflected or converted at the surface of the Earth or at the core-mantle boundary(CMB). Fig. 2.52 depicts a typical collection of possible primary and secondary ray paths together with a three-component seismic record at a distance of D = 112.5° that relates to the suit of seismic rays shown in red in the upper part of the cross section through the Earth. The phase names are standardized and in detail explained in IS 2.1
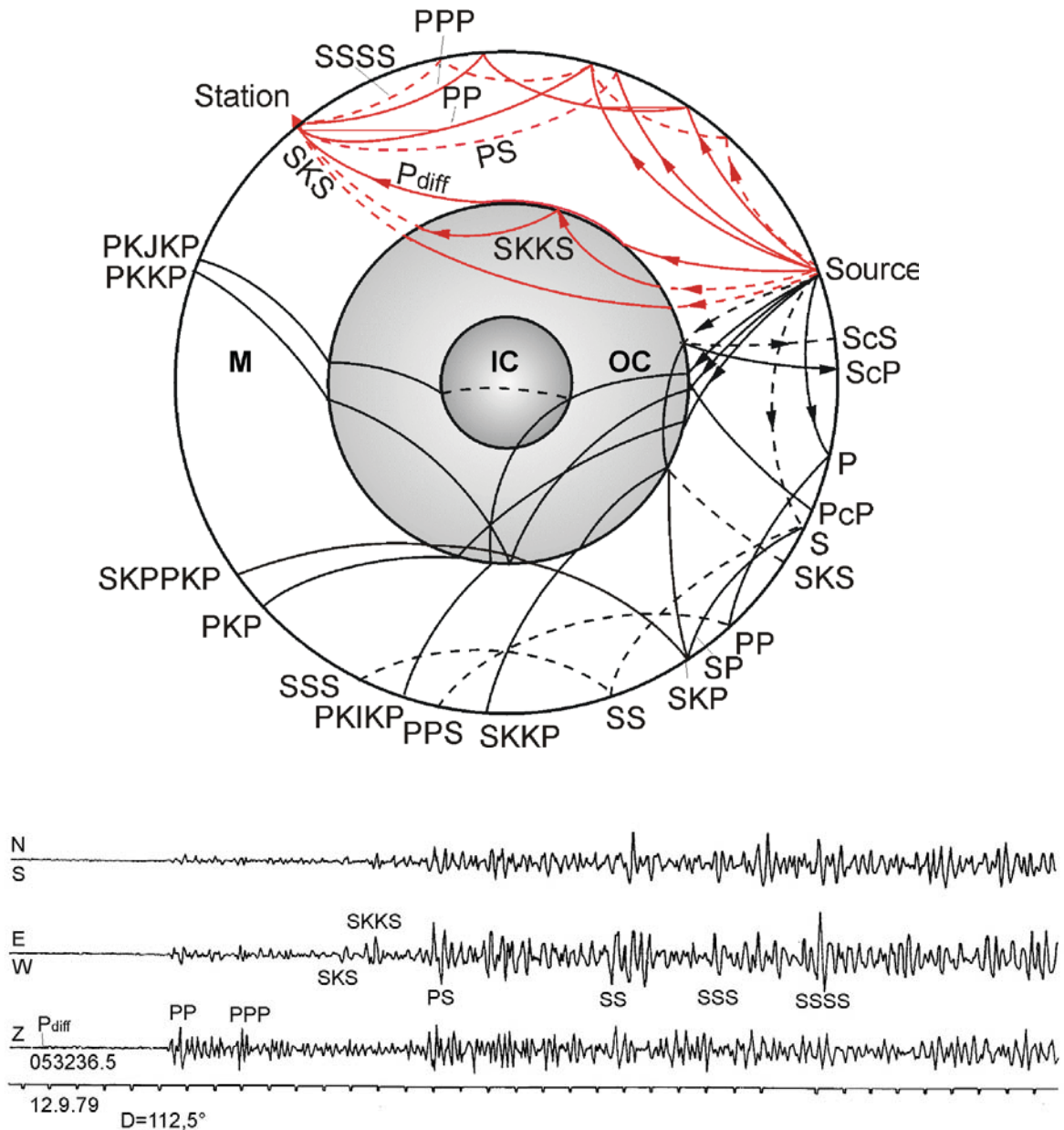

Fig. 2.52 Top: Seismic ray paths through the mantle (**M**), outer core (**OC**) and inner core (**IC**) of the Earth (above) with the respective phase symbols according to the international nomenclature (see IS 2.1, also for detailed ray tracing). Full lines: P rays; broken lines: S rays. Related travel-time curves are given in Fig. 2.60. Red rays relate to the seismic phases identified in the 3-component Kirnos SKD broadband seismogram recorded at station MOX, Germany (**bottom**) of body-waves from an earthquake at an epicenter distance of 112.5°.

Between about 30° and 100° epicenter distance P and S have traveled through the lower mantle, which is characterized by a rather smooth positive velocity and density gradient (see Fig. 2.79). In this distance range, seismograms are relatively clearly structured with P and S (or beyond 80° with SKS) being the first, prominent longitudinal and transverse wave arrivals, respectively, followed by multiple surface and core-mantle boundary (CMB) reflections or conversions of P and S such as PP, PS, SS and PcP, ScP etc. (see travel-time curves in Fig. 2.60).

Within about 15 to 35 min after the first P arrival multiple reflections of PKP from the inner side of the CMB (PKKP; P3KP) or from the surface (PKPPKP = P'P') may be recognizable in short-period seismic records. Their travel-time curves have been plotted in the left-hand panel and their ray traces in the right-hand panel of Fig. 2.53. Many more of such multiple core phase records are presented in Chapter 11, section 11.5.3.
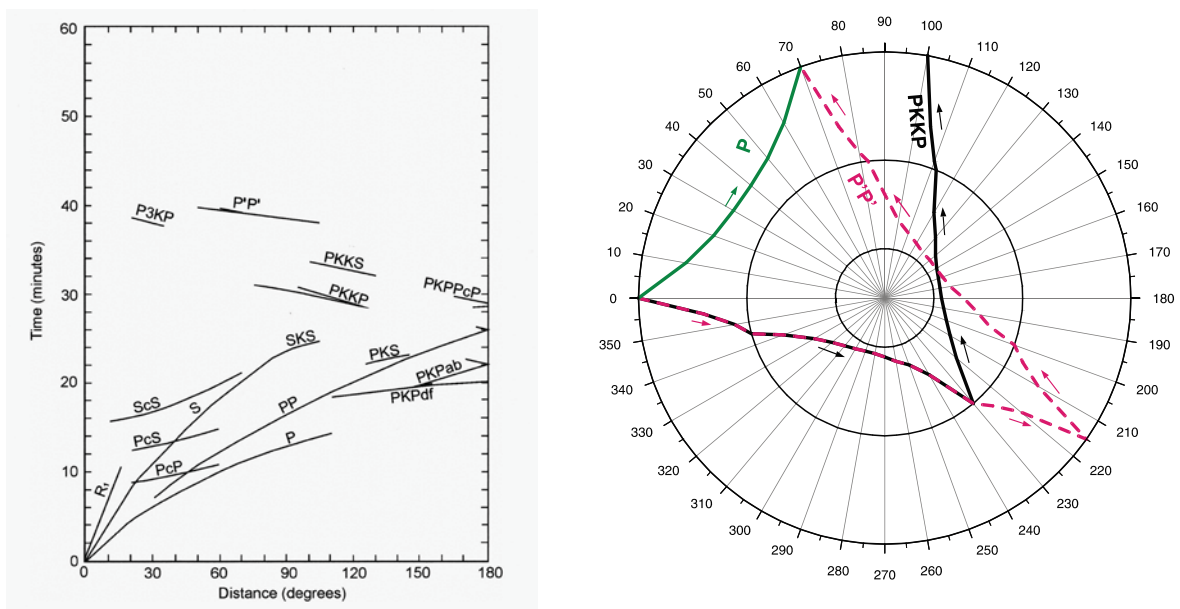

Fig. 2.53 Left: Short-period teleseismic travel-time curves and **right:** ray paths of PKKP and P'P' (= PKPPKP) with respect to the direct P phase (courtesy of S. Wendt, 2001).

Beyond 100°, P-wave rays, which entered the outer core after strong downward refraction, will return with time delay to the surface as PKP core phases (Fig. 2.53 left). This is due to the strong reduction of the P-wave velocity at the CMB from about 13.7 km/s in the lowermost mantle to 8.0 km/s in the upper outer core. Thus, short-period P waves form a *core shadow* whereas PKP forms a caustic around 145° due to the slow velocity increase in the liquid outer core and the strong positive velocity gradient in the transition to the solid inner core (see 2.76). This results in strong amplitudes that are comparable with those of P at much shorter distances around 50° (see Chapter 3, Fig. 3.34). At the caustic of PKP three different branches of PKP meet (see Figs. 2.53 and 2.54 and Chapter 11, Figs. 11.72 and 11.73).
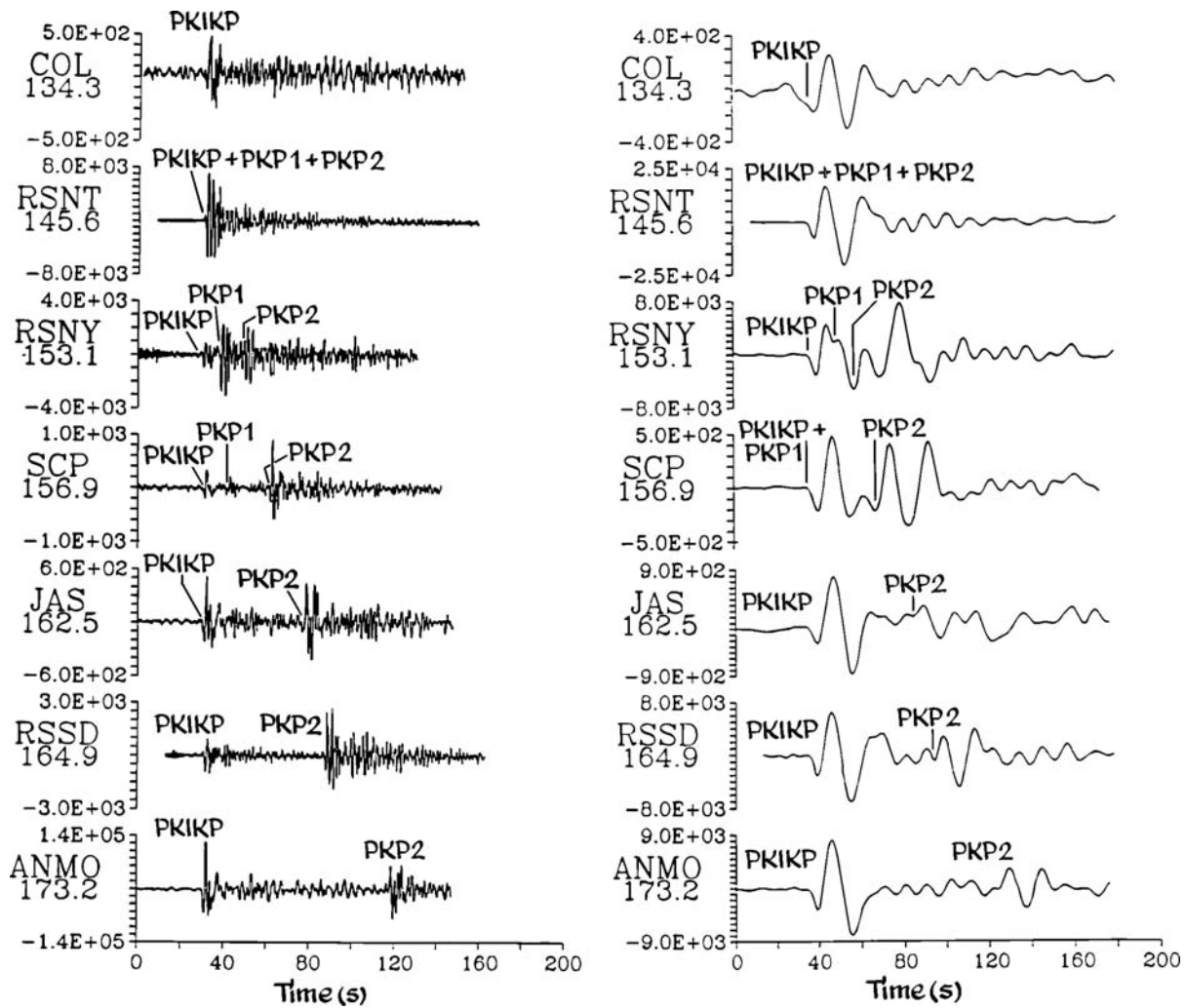
Fig. 2.54 Short-period (left) and long-period (right) seismograms for the Mid-Indian Rise earthquake on May 16, 1985 (M = 6.0, h = 10 km) in the range D = 145.6° to 173.2°. (From Kulhánek (1990), Anatomy of Seismograms, plate 55, pp. 165-166, © with permission from Elsevier Science). Note: The figure above gives still the old names of the core phases. According to the new IASPEI phase names PKP2 should be replaced by PKPab, PKP1 by PKPbc and PKIKP by PKPdf (see IS 2.1, also for the detailed ray tracing of these phases).

Note, however, that long-period P-wave energy is diffracted around the CMB into this shadow zone for short-period P-wave energy up to about 150° (Fig. 2.55). According to the new IASPEI nomenclature of phase names (see IS 2.1) the diffracted P wave is termed Pdif, however the old phase symbol Pdiff is still widely used. The amplitudes of Pdif are much smaller than those of PP, which is the strongest longitudinal arrival in the far teleseismic range (see Fig. 2.55 and Figs. 11.74 and 11.75 in Chapter 11).

In more detail, the types of seismic phases appearing at teleseismic distances and their peculiarities are discussed in Chapter 11, where many additional record examples are given, complemented by Datasheets DS 11.2 and 11.3.
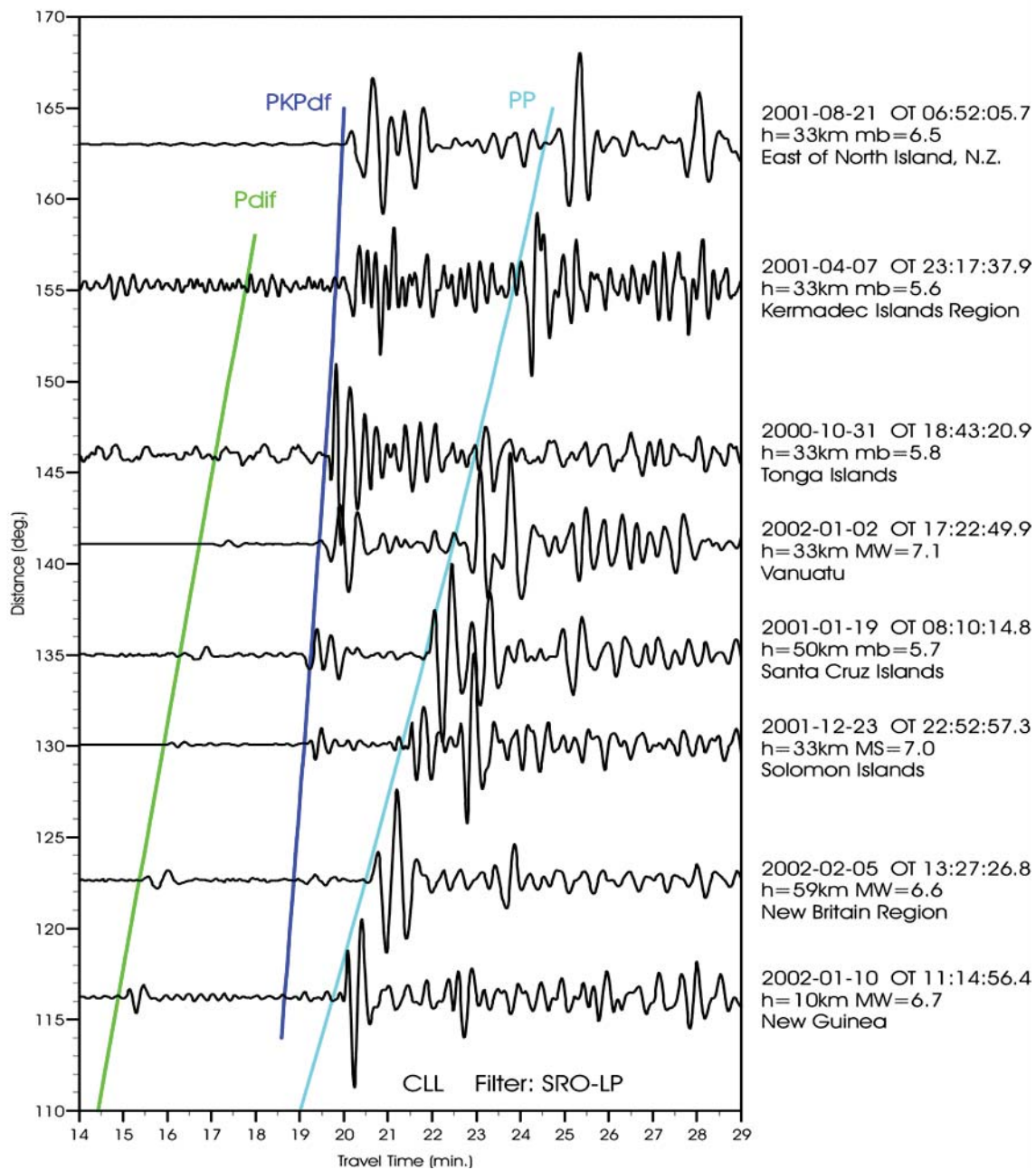
Fig. 2.55 Long-period records of Pdif, PKPdf (with shortly after following PKPbc between 145° and 157° and PKPab (between 145 and 180°; all better discernable in the short-period records of Fig. 2.54), and PP (courtesy of S. Wendt, 2002).

The first discernable motion of a seismic phase in the record is called the *arrival time* and the measurement of it is termed *picking* of the arrival (see Chapter 11, section 11.2.2). Up to now, arrival time picking and reporting to international data centers is one of the major operations of data analysts or automatic analysis systems at seismic stations or network centers. By plotting the time differences between reported arrival times and calculated origin times over the epicenter distance, seismologists were able to construct travel-time curves for the major phases and to use them to infer the average radial velocity structure of the Earth (see 2.7).

In Fig. 2.56 (left) more than five million travel-time picks, archived by the International Seismological Centre (ISC) for the time 1964 to 1987, have been plotted. Most time picks align nicely to travel-time curves, which match well with the travel-time curves theoretically calculated for major seismic phases on the basis of the IASP91 model (Fig. 2.56 right).
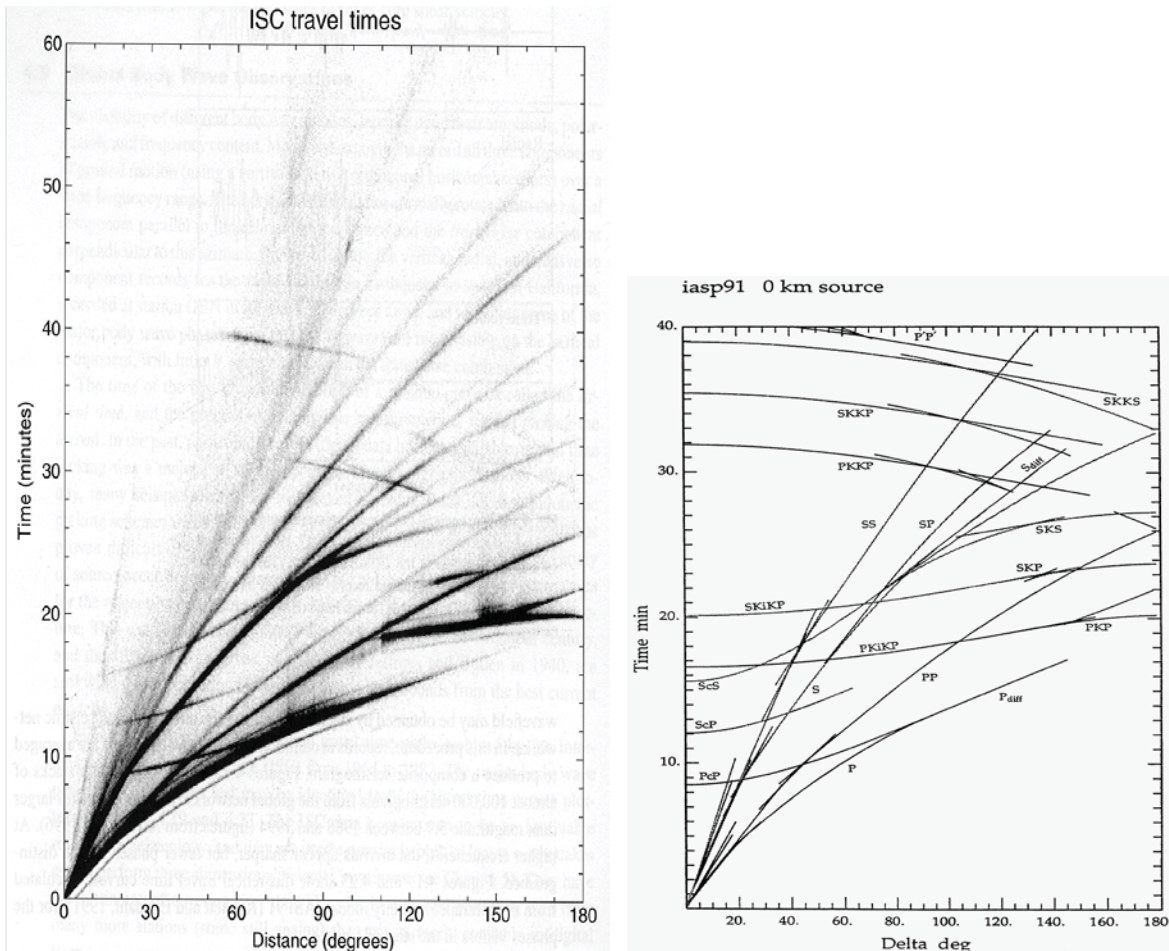

Fig. 2.56 **Left:** Travel-time picks collected by the ISC between 1964 and 1987 for events shallower than 50 km. (From Shearer, Introduction to Seismology, 1999; © with permission from Cambridge University Press). **Right:** IASP91 travel-time curves for surface focus (from Kennett, 1991).

An even more complete picture of the entire seismic wavefield may nowadays be obtained by stacking data from global digital seismic networks. Records at common source-receiver ranges have been averaged to produce a composite seismogram. Stacks of almost 100,000 seismograms from the global digital networks have been plotted by Astiz et al. (1996; Fig. 2.57 for short-period records with periods T < 2s and Fig. 2.58 for long-period records with T > 10 s). Although the arrivals appear sharper at higher frequencies and late arriving reflected core phases P'P' (PKPPKP), PKKP as well as higher multiples of them are discernable in short-period records only, in total much less later phases can be distinguished in short-period records. The darker the dot "curves" appear against the gray background the larger is the relative frequency with which these phases can be observed above the noise level. Figs. 2.59 and 2.60 present the calculated travel-time curves for the IASP91 velocity model (Kennett and Engdahl, 1991) together with the phase nomenclature. The theoretical travel-time curves match excellent with the difference between automatically picked onset times and origin time.
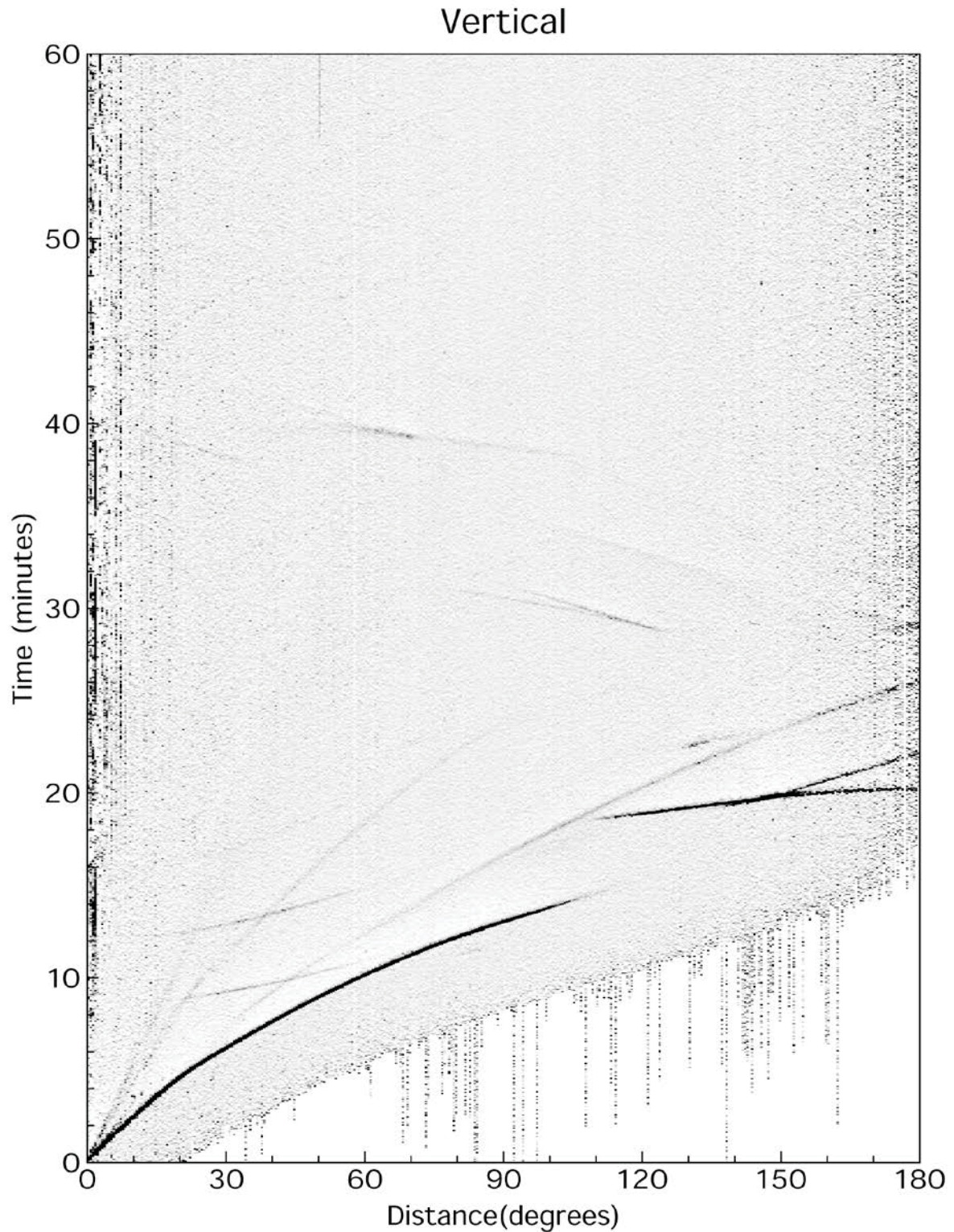
Fig. 2.57 Stack of short-period filtered (T < 2 s), vertical component data from the global networks between 1988 and 1994 (from Astiz et al., Global Stacking of Broadband Seismograms, Seismogical Research Letters, Vol. 67, No. 4, p. 12, © 1996; with permission of Seismological Society of America).
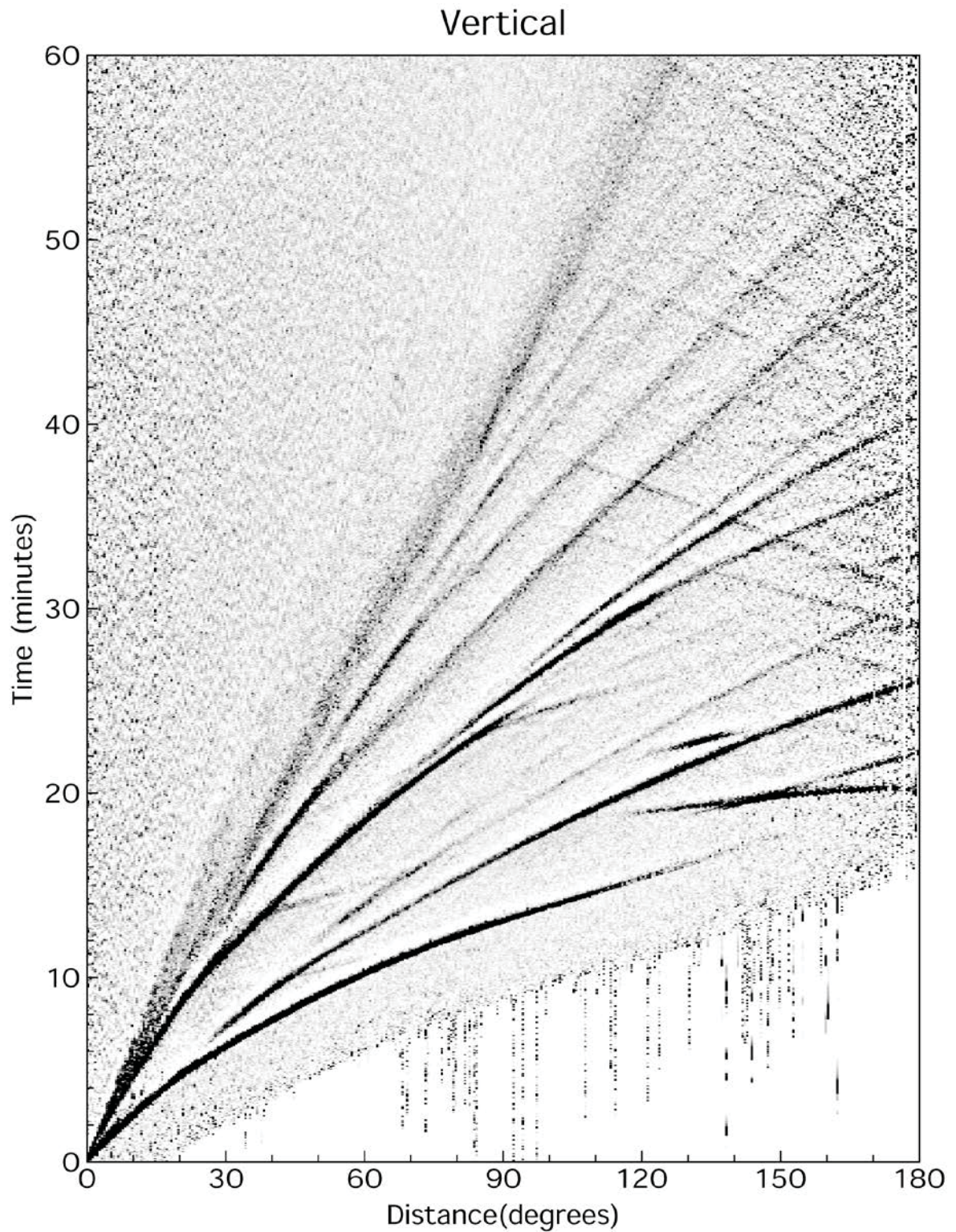
Vertical

Fig. 2.58 Stack of long-period (T > 10 s), vertical component data from the global networks between 1988 and 1994. (from Astiz et al., Global Stacking of Broadband Seismograms, Seismological Research Letters, Vol. 67, No. 4, p. 14, © 1996; with permission of Seismological Society of America).
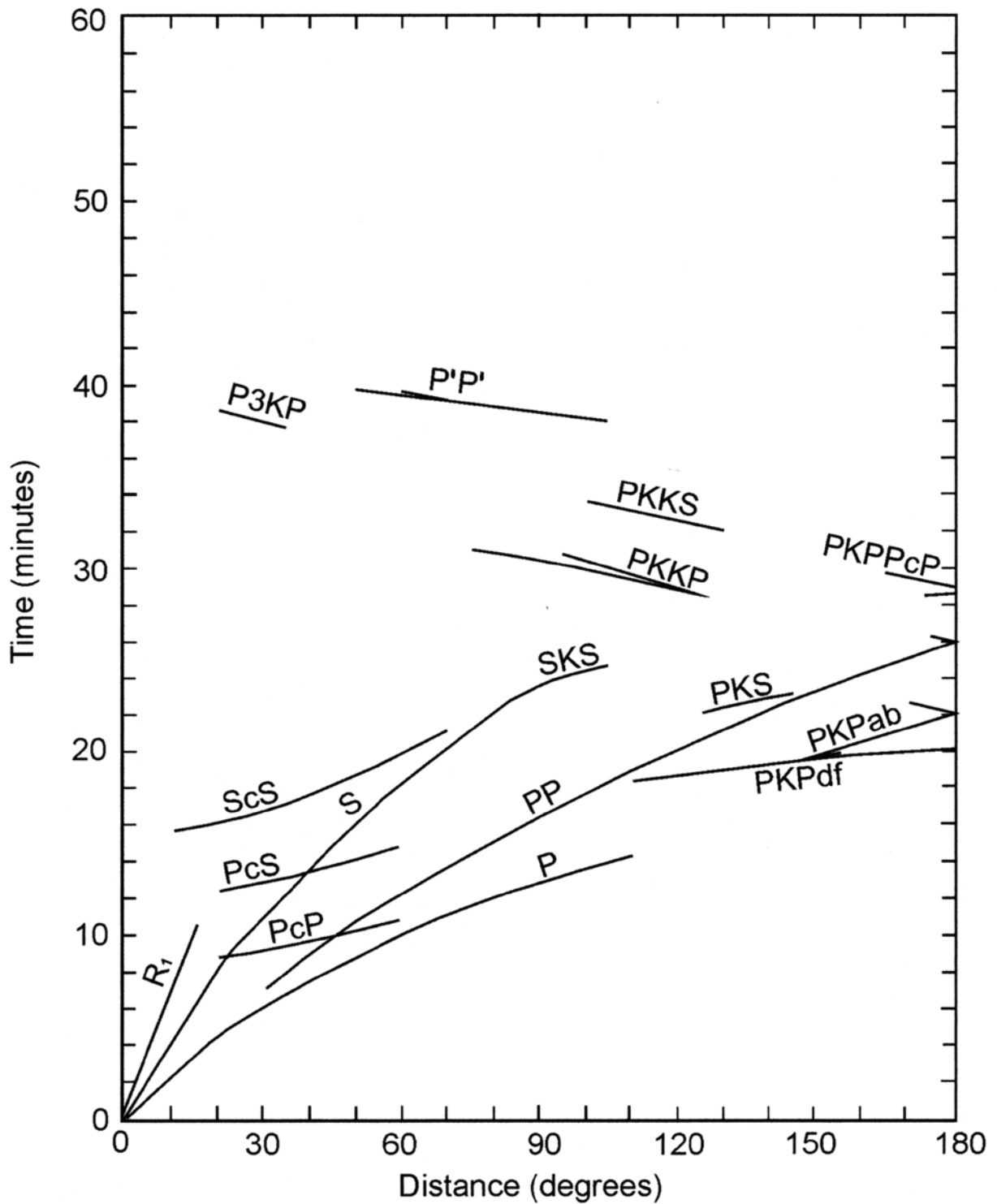
Fig. 2.59 Overlay to Fig. 2.57 with the theoretical IASP91 travel-time curves for surface foci and the related phase nomenclature. Produce a 1:1 copy on a transparent sheet and match it with Fig. 2.57.

Fig. 2.60 Overlay to Fig. 2.58 with the theoretical IASP91 travel-time curves for surface foci and the related phase nomenclature. Produce a 1:1 copy on a transparent sheet and match it with Fig. 2.58.
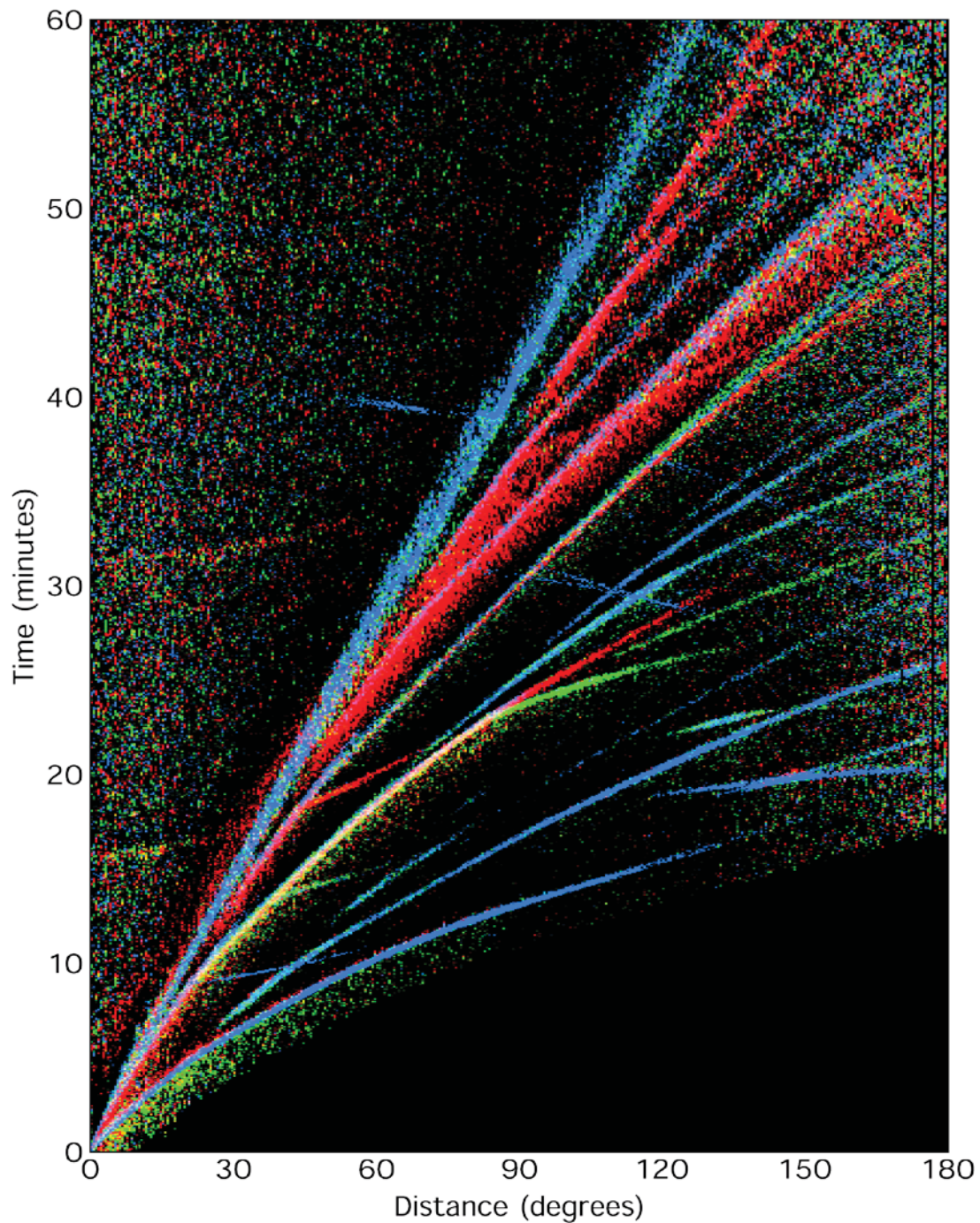
Complementary to Figs. 2.57 and 2.58, Fig. 2.61 reveals the different polarization of the various seismic phases.

Fig. 2.61 Global travel-time curves for shallow earthquakes as produced by stacking broadband seismograms. Seismic phases are shown in different colors depending on their polarization (**blue:** vertical motion; **green:** radial-horizontal; and **red:** transverse-horizontal) (courtesy of L. Astiz).

While all primary longitudinal phases and all from P or K to S converted phases, and vice versa, appear on vertical and radial-horizontal components only, multiple reflected S waves, which lose with each reflection more and more of their SV polarized energy due to conversion into P (or K at the CMB), become more and more transversely polarized. Primary

S, however, has significant energy on both horizontal components that are oriented either parallel to the backazimuth to the source (radial) or perpendicular to it (transverse). Direct P waves, polarized in the direction of ray propagation, have in the teleseismic range dominating vertical components because of their steep incidence angle, which gets smaller and smaller with increasing distance (see e.g., PKP phases). PP, P3 and higher multiples may, however, have significant energy in the radial component too. These examples illustrate that the visibility and discrimination of body wave phases in seismic records depends on their relative amplitude, polarization and frequency content. All of these criteria have to be taken into account, besides the differences in travel-times, when analyzing seismic records.

2.6.3 Depth phases

In the case of distant deep earthquakes the direct P wave that leaves the source downward will arrive at a teleseismic station first. It will be followed, depending on the source depth, up to about 4.5 min later, by other phases that have left the source upward (Fig. 2.62). These phases, also when associated with PP, S, SS and reflected or converted at the free surface of the Earth or at the ocean bottom (such as pP, sP, ', sPP, pPKP, etc.), at the free surface of the ocean (e.g., pwP, swP), or from the inner side of the Moho (e.g., pm-P) are called *depth phases*. Their proper identification, onset-time picking and reporting is of crucial importance for reliable determination of source depth (see below and section 6.1 with Figure 7 in the Information Sheet IS 11.1). Differential travel-time tables for pP-P and sP-P are presented in Exercise EX 11.2. For the definition of these phases see also IS 2.1.
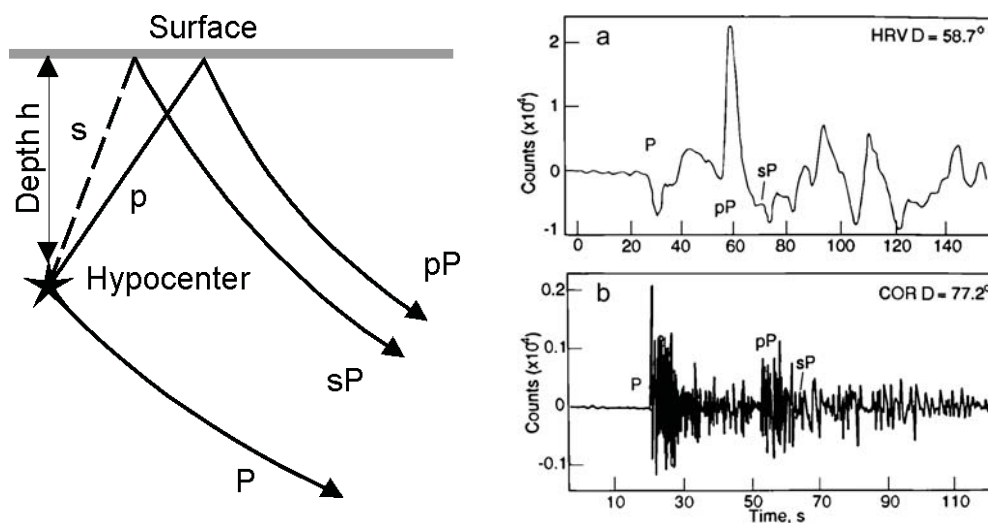

Fig. 2.62 Left: Different ray paths of a direct teleseismic P wave and of its depth phases. **Right:** Records of depth phases of the May 24, 1991 Peru earthquake (hypocenter depth h = 127 km); a) broadband record and b) simulated short-period recording (the right figure is a corrected cutout of Fig. 6.4 of Lay and Wallace, Modern Global Seismology, p. 205, © 1995; with permission of Elsevier Science, USA).

Depth phases of P, PP, S, SS or of converted P or S phases have commonly smaller amplitudes because of reflection and/or conversion losses as well as extra attenuation along the additional segment of travel. For shallow earthquakes a clear discrimination between

direct and depth phases is difficult and usually beyond the possibilities of routine seismogram analysis because of the closeness in time of the subsequent phase onsets and the superposition of their waveforms. They may, however, be discriminated by waveform modeling and matching for variable source depth and source mechanism (see subchapter 2.8, Fig. 2.85). Yet, in any event, for shallow earthquakes, short-period seismic records that emphasize on periods < 2-3 s are more suitable for identifying and time-picking of closely spaced depth phase onsets than broadband displacement or (somewhat better) velocity records (Fig. 2.63).
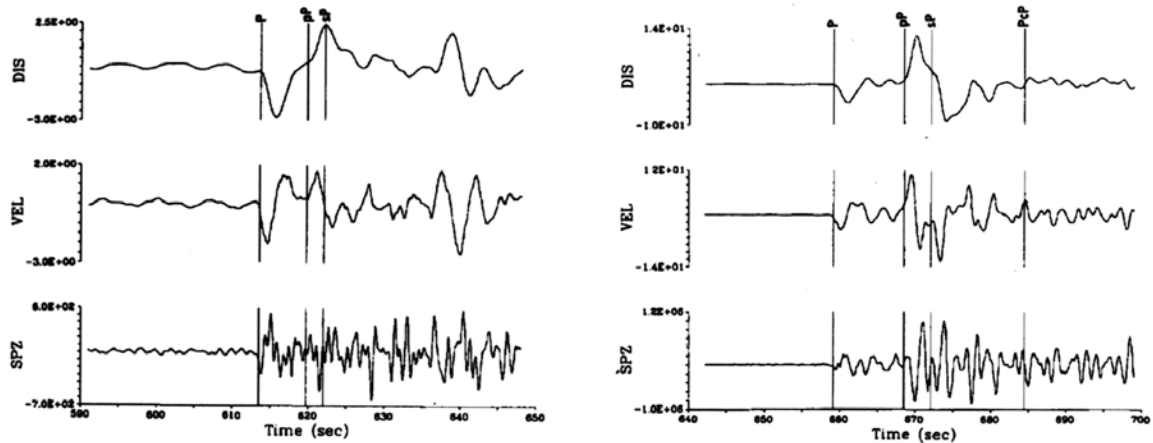

Fig. 2.63 Appearance of P, pP and sP in displacement (DIS) and velocity (VEL) broadband as well as short-period vertical component records. The source depths of the earthquakes have been 18 km (left) and 40 km (right), respectively. Copied from Figures 1 and 5 in Choy and Engdahl (1987), Phys. Earth Planet. Int. **47** (© Elsevier Science Publ., 2012).

Yet, depth phases may sometimes also be larger than their primary phases, as confirmed by both observations (e.g., Fig. 2.62 upper right, Fig. 2.63 right and 2.64 below) and synthetic modeling (e.g., Langston and Helmberger, 1975).
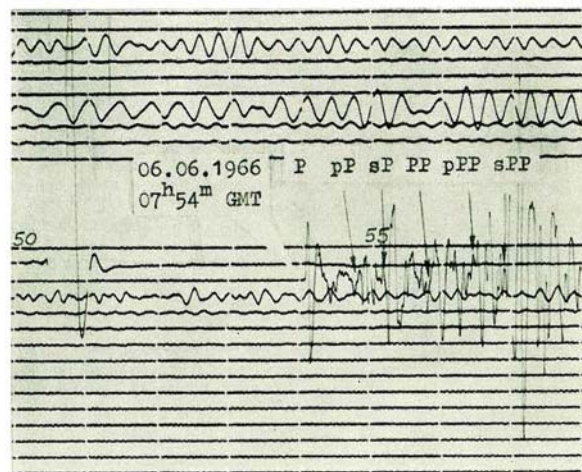

Fig. 2.64 Medium-period displacement-proportional record of P, PP and their depth phases by a Kirnos SKD seismograph (T_s = 20s; T_g = 1.25 s; V_{max} = 1000 times) at station MOX, Germany, of an earthquake in the Afghanistan-USSR border region on 06 June 1966 (D = 44.3°, h = 220 km). Copy of Fig. 7 in Bormann (1969).

The great variability of amplitudes of both P and PP (also S and SS) and of their depth phases is a source-mechanism dependent function of take-off angle and azimuth and thus varies with distance and azimuth of the recording station in respect to the source radiation pattern.

Although the inclusion of correctly identified depth phases into the location procedure (besides S, PKiKP, PKPdf, PcP, ScP, if available) may significantly improve hypocenter location their proper identification becomes even more difficult if the reflection/conversion points of the up-going p or s rays are underneath an ocean with significant water depth. In this case significant reflection/conversion may occur both at the ocean bottom and at the ocean surface. While the former would be the common pP or sP phase, the latter requires a specifying phase name, namely pwP or swP (w = water). There maybe even double reflections within the water column, making, e.g., for a pwwP (see Fig. 2.65).
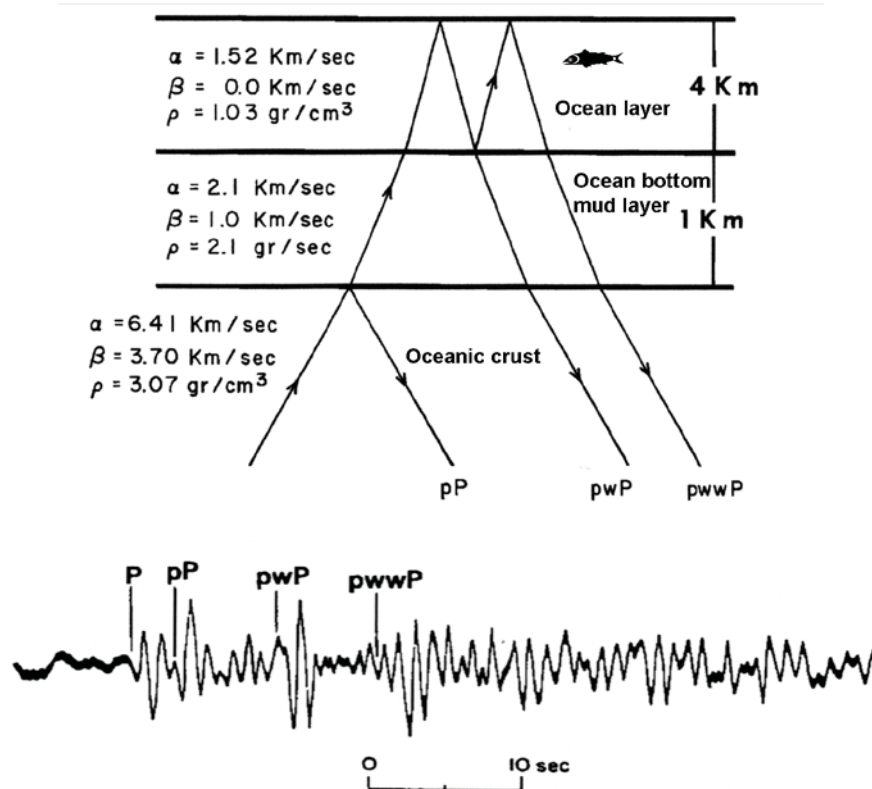

Fig. 2.65 **Top:** Average crust-ocean layer velocity model with seismic rays of P and its depth phases (amended after Mendiguren, 1971). **Bottom:** A short-period record example of theses phases according to Engdahl and Billington (1986).

These ocean depth phases have first been described by Mendiguren (1971) and later in more detail by Yoshiu (1979) and Engdahl and Billington (1986). Since the water layer depth phases follow the primary depth phases usually within about 10-15 s, their waveforms are better discernable and their onset times more reliable to pick on short-period or velocity broadband records than on long-period or displacement broadband records (Fig. 2.66).
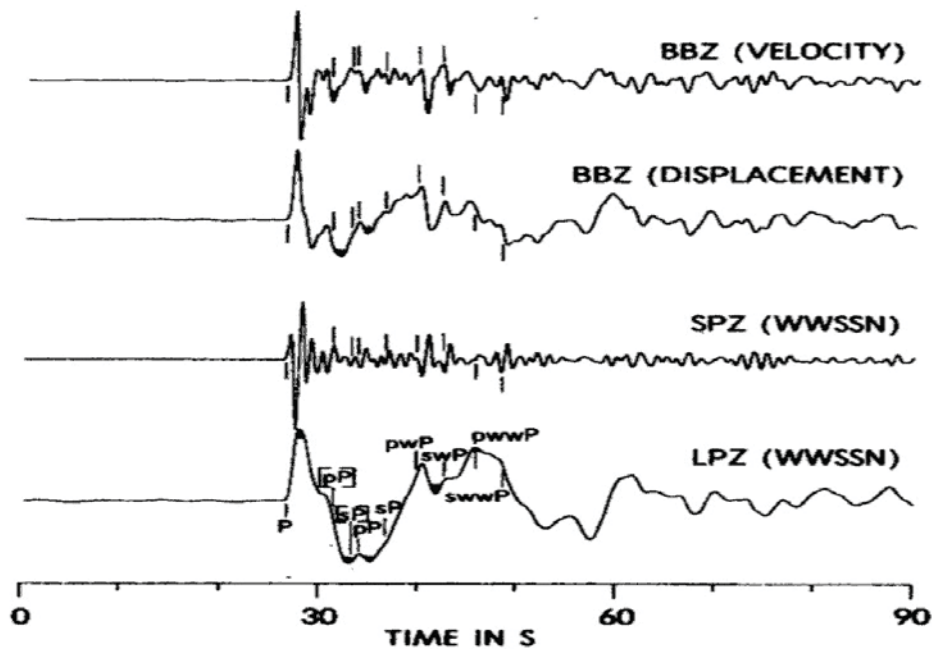
Fig. 2.66 P and the depth-phase reflections from the oceanic sediment-basement interface ([pP] and [sP]), from the sediment-water interface (pP and sP), from the water surface (pwP and swP), as well as the multiples of the latter, once again reflected within the water layer (pwwP and swwP) (see Fig. 2.65 top), recorded with different instruments. Vertical bars mark the model-dependent theoretically calculated onset times of these phases. The figure was modified for better time-resolution from Figure 3b in Engdahl and Kind (1986), Annales Geophysicae, **4,** (© European Geophysical Society, 2012).

According to the record examples shown, the water-layer depth phases may be even larger than the primary depth phases. Misinterpretations are therefore rather common. About one-third of the ISC identifications as pP, sP and PcP have been re-identified in a special analysis carried out by Engdahl et al. (1998). According to these authors quite many ISC pP, sP and partially also PcP phases have in fact been pwP and many sP onsets had been misinterpreted as pP. If a pwP phase produced by a water layer 4 km thick is misinterpreted as pP this may result (in the absence of local or regional P phases) in an overestimation of the focal depth by about 50 km. Therefore, Engdahl et al. (1998) developed an automatic phase identification algorithm, termed EHB for short, which aims at significantly improved hypocenter relocations. EHB is applied to the phase group which immediately follows the P phase at teleseismic distances, including pP, pwP, sP and PcP and allows the unambiguous identification of later phases such as S. In conjunction with there publication the authors relocated some 100.000 earthquakes. The EHB bulletin is now permanently updated and complemented and posted on the ISC website http://www.isc.ac.uk/.

2.6.4 Pz ± P, Sz ± S, Pz ± S, Sz ± P, etc.

Since the *impedance contrasts* at the free Earth surface, the ocean bottom and the core-mantle boundary are larger than at any other velocity-density discontinuity in the Earth, reflected and converted P and S phases from these discontinuities dominate the secondary body-wave onsets in seismograms. None the less, there are several other globally represented

73

discontinuities of significant contrast which give rise to additional reflections and conversions of P and S phases which may appear even in unprocessed seismograms as recognizable fore- or after-runner onsets to the primary phases P and S and thus complicate for analysts the proper phase identification and onset picking. The most important discontinuities in this regard are the Moho as well as the discontinuities bordering the upper mantle transition zone at about 410 km and 660 km depth. According to IS 2.1 as well as Storchak et al. (2003 and 2011) the unified nomenclature for such phases is:

• **Pz+P or Sz+S:** P or reflection from the **outer** (top) side of a discontinuity at depth z outside of the core; z may be a positive numerical value in km, e.g., P660+P or S660+S, which are then reflections of P or S from the top of the 660 km discontinuity, or z may be a letter, e.g., m for Moho (see Pm+P and the bottom side reflection pm-P in Fig. 2.67).
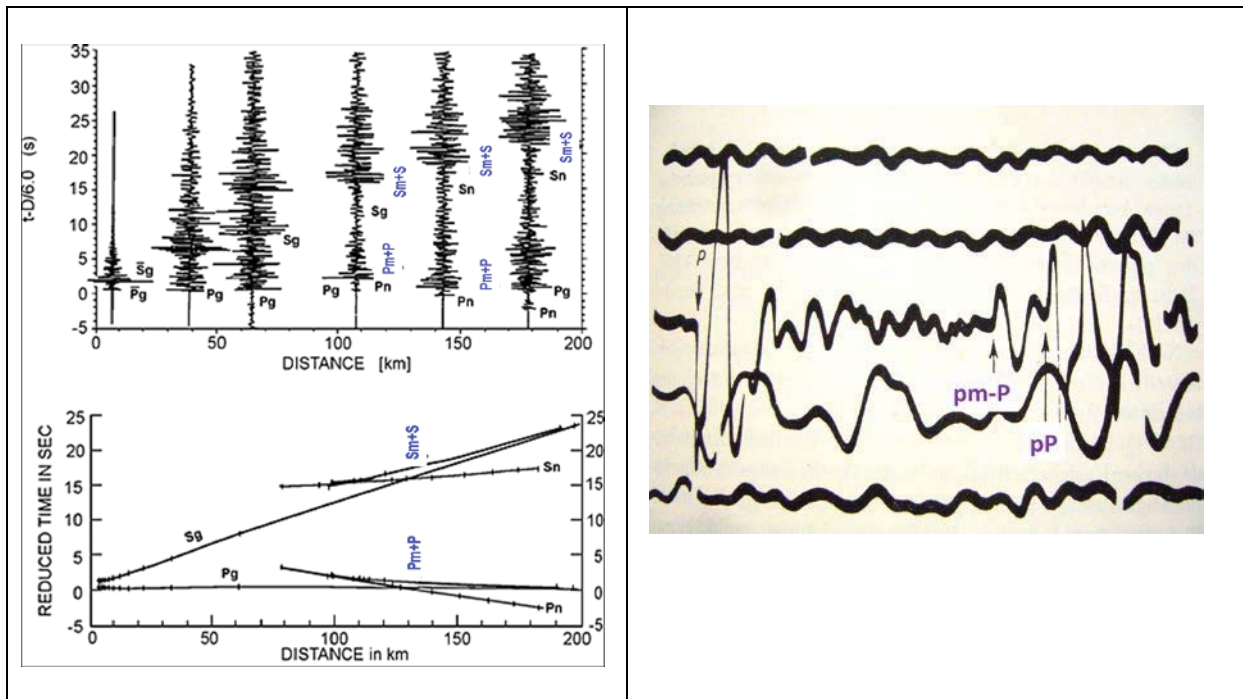

Fig. 2.67 Left: Travel-time curves and records of critically reflected crustal P and S waves from the upper side of the Moho: Pm+P and Sm+S, respectively. **Note:** The +sign is not obligatory to identify the phase as on upward reflection from the upper side of a discontinuity. Writing PmP and SmS instead is acceptable. See IS 2.1. Modified from Fig. 2.47;
Right: Depth phase pP from an earthquake at the Tyrrhenian Sea (13.04.1938, h = 256 km) recorded at the station Sverdlovsk, Russia (D=33°), together with its smaller forerunner phase pm-P which is the downward reflection of the upcoming ray p on the inner (bottom) side of the Moho (**see next bullet point**). Modified Figure 108 in Savarenski and Kirnos (1960).

• **Pz-P or Sz-S:** P or S reflection from the **inner** (bottom) side of a discontinuity at depth z outside of the core, e.g., at the Moho (see Fig. 2.67 right) or in the Earth upper mantle such as P660-P or S410-S which are the P or S reflections from below the 660 km and 410 km discontinuity, respectively, and **precursory to PP or SS** (Fig. 2.68 and 2.69). **Note:** Writing the -sign is in these cases obligatory to identify them as a downward reflections from the bottom side of the discontinuity.
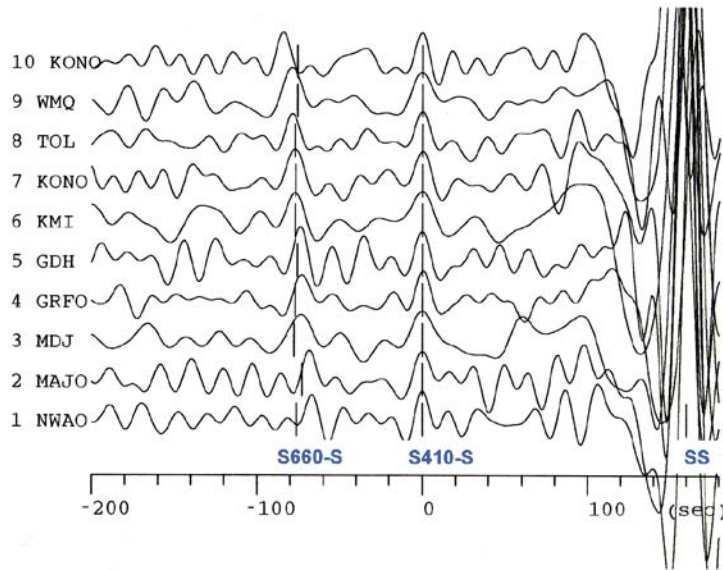
Fig. 2.68 Aligned long-period records of SS phases (very large amplitudes on the outermost right) and of their much weaker precursors reflected from the inner (bottom) side of the discontinuities in the mantle at 410 km **(S410-S)** and 660 km **(S660-S)** depth from different earthquakes recorded at different seismic stations and distances: Trace 1: 1983 Oct 17 19:36:21.5 ; Trace 2: 1980 Jan 27 16:38:01.1; Trace 3: 1988 Feb 06 18:03:54.8; Trace 4: 1980 Oct 25 11:00:05.1; Trace 5: 1990 Feb 19 05:34:37.4; Trace 6: 1990 Dec 17 11:00:19.6; Trace 7: 1989 Apr 18 12:33:54.8; Trace 8: 1984 May 26 22:42:47.3; Trace 9: 1989 Dec 03 14:16:48.8; Trace 10:1986 Jun 28 05:03:47.5. The vertical bars mark the theoretical travel times with respect to S410-S according to the global IASP91 model. Modified after Gossler and Kind (1996).
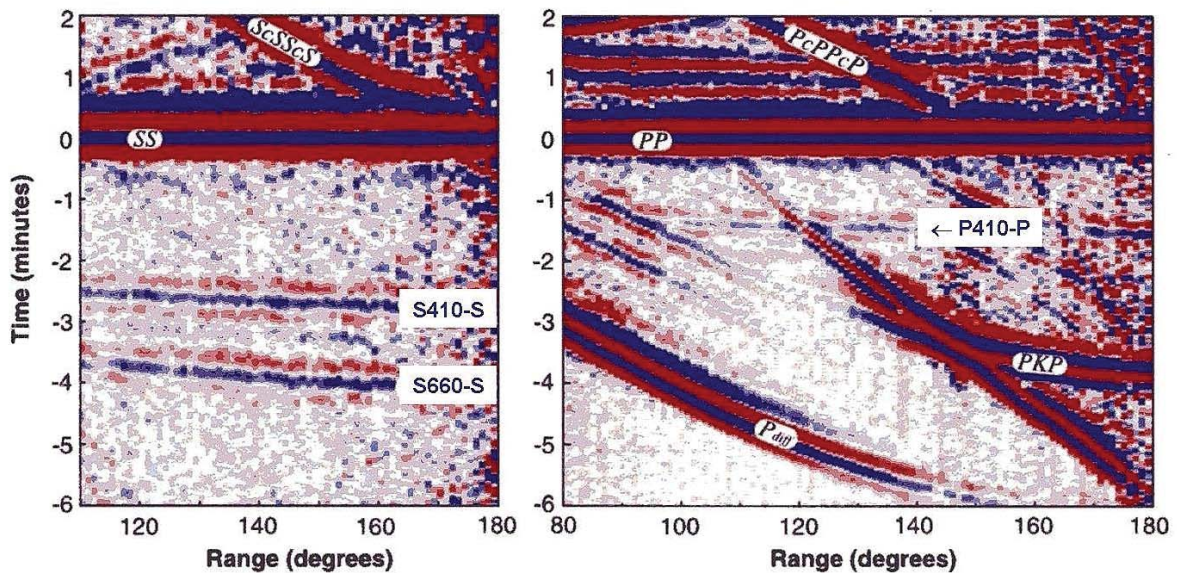

Fig. 2.69 Left: Similar to Fig. 2.68 but stacked and **c**olor-coded record section in a wide distance range, and aligned with respect to the arrival time of the free surface reflection of SS. Clearly visible are the fainter precursory arrivals of S660-S and S410-S, which arrive about 4 and 2.5 min ahead of the SS. **Right:** The same for the still weaker P410-P with respect to PP. Modified from Figure 1 in Shearer and Flanagan (1999), Science, **285**, p. 1546, in order to agree with IASPEI standard phase nomenclature (© Science).

• Accordingly, Pz+S and Sz+P or Pz-S and Sz-P, respectively, are P or S waves that have been converted into S or P when reflected from the outer (top) or inner (bottom) side, respectively, of a discontinuity at depth z.

• In an analog way the above notations apply also to PKP = P' and SKS = S' phases, such as P'z-P' being a PKP phase reflected from the inner (top) side of a discontinuity at depth z outside the core, thus being precursory to P' = PKP. A fine example is given in Fig. 2.70.

Usually, however, the SNR of such phases is too small to be recognized and picked correctly in routine seismogram analysis.
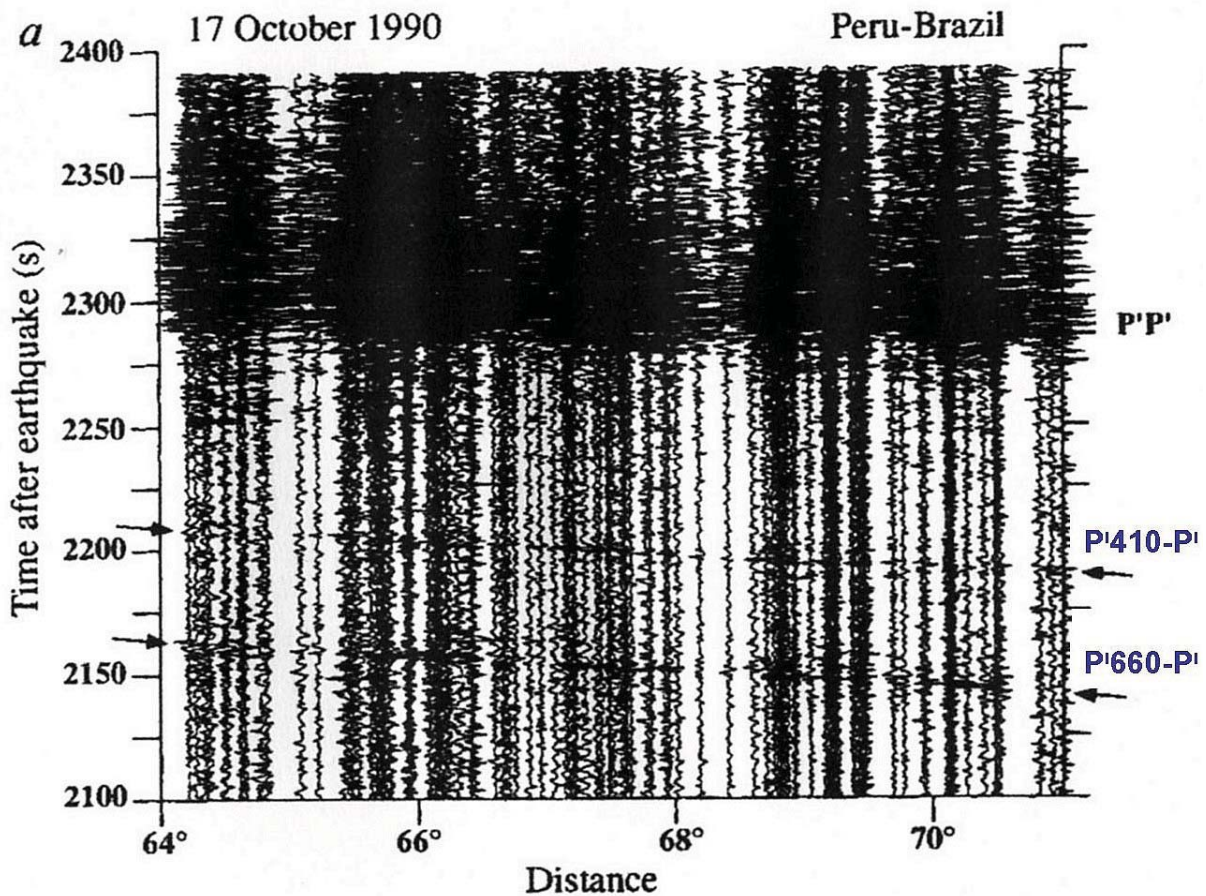

Fig. 2.70 P'P' record section for a South American earthquake recorded by the California seismic array showing weak but distinct precursors P'P' and P'P'. Modified from Fig. 2a of Benz and Vidale (1993), Nature, **365**, p. 148, in order to agree with IASPEI standard phase nomenclature. (© Copyright Clearing Centre of Nature).

2.6.5 T phases

The letter *T* stands for *Tertiary wave*. This term has been introduced into seismology by Linehan (1940) in order to discriminate these waves from the much earlier arriving P (primary) and S (secondary) waves radiated by the seismic source that have travelled all their way through the Earth. T waves are generated by earthquakes, explosions or volcanic eruptions in or near the oceans, propagate in the oceans as an acoustic wave guided in the

SOFAR channel (Bullen and Bolt, 1985) or by multiple reflections between the sea floor and the sea surface (Båth and Shahidi, 1974) and are converted back to seismic waves at the ocean-land boundary near the recording site. The SOFAR channel is a depth range of low acoustic velocity within the ocean water column which "traps" sound waves to propagate over very large distances with very low attenuation. Thus it is a very efficient *wave guide* for the seismic *T phase*. T waves are generally short-period waves because they can propagate efficiently only, if their wavelengths fit inside the width of the SOFAR channel. This is the case for frequencies above 2 Hz only (see Okal et al., 2003, and records in Figs. 2.71 and 2.72). T waves are best recorded by ocean-bottom seismometers (OBS) and hydrophone stations (see Chapter 7, section 7.5) and by near coastal inland stations. Typical for T phases is their gradual increase and subsequent decrease of the amplitudes of rather monochromatic oscillations with a total duration up to several minutes and hardly any recognizable onset time (see the markers ET set in Fig. 2.71).

Since T phases travel through the SOFAR channel with much lower velocity than the direct P and S waves radiated by the seismic source, the T phases arrive much later in the seismic record, the later the longer the SOFAR path. Therefore, they may be misinterpreted as independent seismic events. Figs. 2.71 and 2.72 present T-phase records at stations of the Norwegian National Seismic Network from two earthquakes in the Atlantic Ocean.
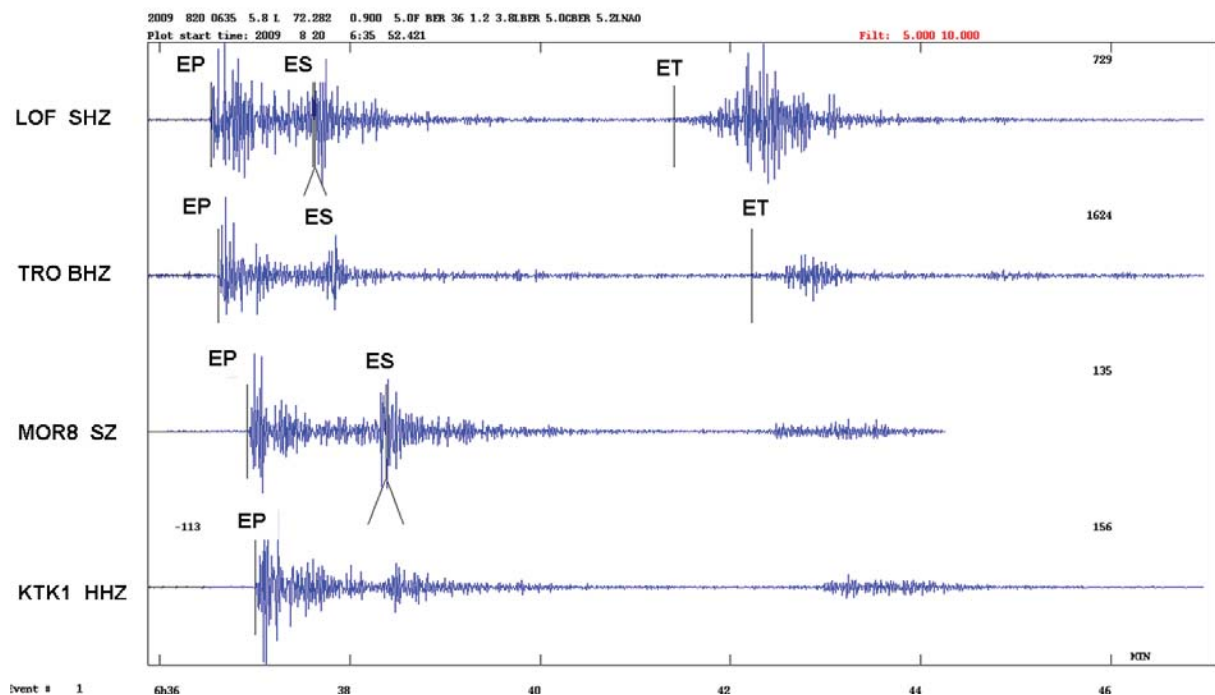

Fig. 2.71 High-frequency filtered records (passband 5 to 10 Hz) at stations LOF, TRO, MOR8 and KTK1 in Norway of the shallow (h = 5 km) Ml = 5.2 Mohns Ridge earthquake on 20 Aug. 2009. Note the at least some 2 minutes long gradual T phase with no clearly recognizable onset ET which follows about 4 to 5 min after the first P onset. The epicenter distance of the stations and their distance from the coast (second number in brackets) are – from top to bottom - for LOF 730 km (15 km), TRO 710 km (30 km), MOR8 860 km (100 km) and KTK1 900 km (200 km). (Modified version of an original record plot kindly provided by Lars Ottemöller, 2011).

.

Although the amplitudes of the primary and secondary earthquake waves in all 4 records are about the same, the T-phase amplitudes decrease strongly with increasing distance from the coast due to the rather strong attenuation of the high-frequency waves travelling through the rather heterogeneous uppermost crust. This, however, is not a strict rule, obviously modified by differences in the efficiency of the conversion of the acoustic SOFAR channel waves into seismic waves at the coastal bounce point as well as differences in the attenuation conditions along the travel paths on land. In the second record example in Fig. 2.72, e.g., the T-phase amplitudes recorded on station KTK1 at a coastal distance of 220 km are larger than those recorded on stations TRO and HAMF at 30 km and 75 km coastal distance, respectively.
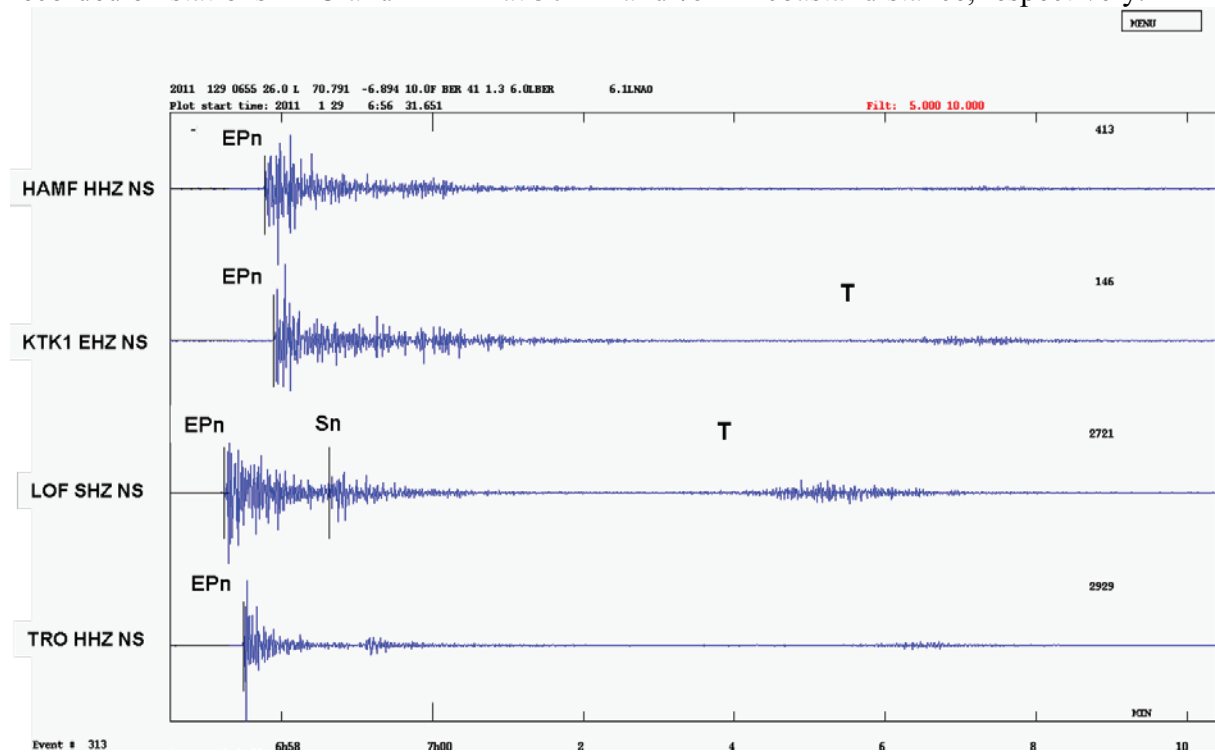

Fig. 2.72 High-frequency filtered records (passband 5 to 10 Hz) at stations HAMF, KTK1, LOF, and TRO in Norway of the shallow (h = 10 km) Ml = 6.1 Jan Mayen region earthquake on 29 Jan. 2011. Note the up to about 4 min long T phase which follow about 6 to 8 min after the first P onset. The epicenter distance of the stations and their distance from the coast (second number in brackets) are – from top to bottom – for HAMF 1115 km (75 km), KTK1 1165 km (220 km), LOF 845 km (15 km), TRO 970 km (30 km). (Modified version of an original record plot kindly provided by Lars Ottemöller, 2011).

As compared to ordinary sub-marine and *tsunamigenic earthquakes*, high-frequency T waves are highly deficient (by 1.5 to 2.5 orders of magnitude) in records of very slow rupturing *tsunami earthquakes*. Therefore, Okal et al. (2003) suggested that computations of T-phase efficiency might become a valuable contribution to real-time tsunami warning in the far field.

2.6.6 Surface-wave fundamental and higher modes and the W phase

The basic types of horizontally propagating seismic surface waves (Rayleigh waves, Love waves, and their higher modes; see 2.3 in Chapter 2) remain more or less unchanged with growing distance. Surface waves, however, do not form seismic phases (wavelets) with well-

defined onsets and duration but rather dispersed wave trains (see Figs. 2.12, 2.13, 2.20). Due to the dispersion their duration increases with distance. Although it is very common to determine the magnitude of shallow seismic events by means of surface waves (Ms_20 and Ms_BB; see Chapter 3 and IS 3.3), the analysis of surface-wave group and phase velocities for investigating Earth structure and properties requires specific methods of analysis and is beyond the scope of seismological observatory practice. Moreover, the phenomenology of seismic surface-wave trains is sometimes complicated by near surface heterogeneities. E.g., surface wave trains of relatively high frequencies, as generated by shallow local events, may additionally be prolonged significantly due to lateral reverberations when propagating through strong lateral velocity contrasts in the crust (see Fig. 2.73). This phenomenon was used by Meier et al. (1997) to establish a tomography with reflected surface waves.
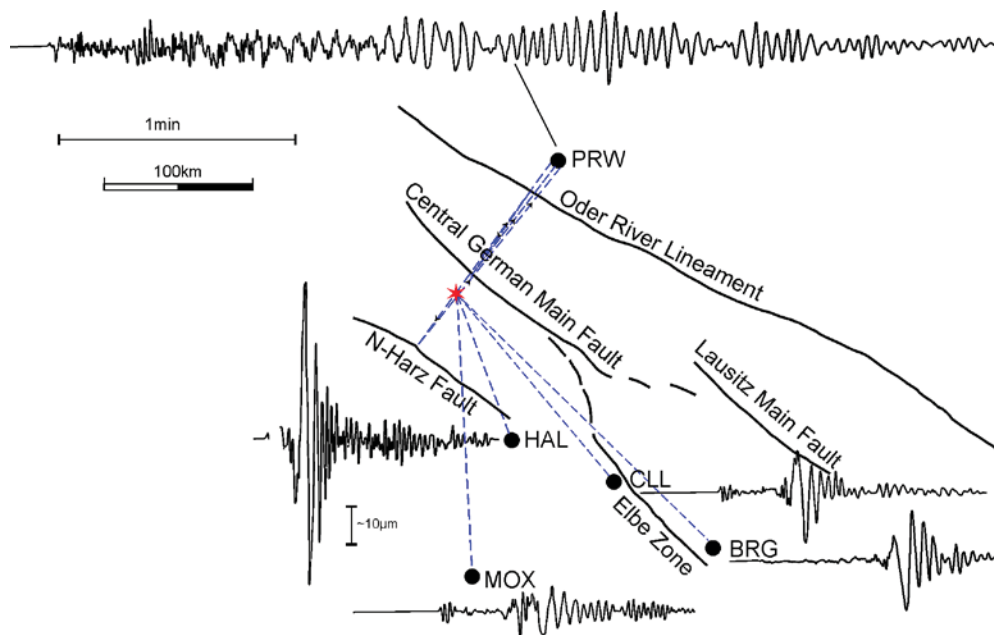

Fig. 2.73 Ray paths of surface waves (broken lines) from a mining collapse (star) to several seismic stations in the eastern part of Germany. Note: Records at stations along travel paths that have not or only once crossed some of the main tectonic faults in the area, are rather short. They have only one surface-wave maximum. In contrast, at station PRW, which is at the same epicenter distance as HAL, the seismic record is about four times longer and shows four surface-wave groups due to multiple reflections at several pronounced fault systems (compiled from data provided by H. Neunhöfer (1985; and personal communication)).

Recently, the analysis of the long-period *W phase*, which arrives before the onset of S (Fig. 2.74), has gained immense practical importance for speeding up seismic tsunami warning. Kanamori (1993) has been first to name and extensively document this phase. According to Kanamori and Rivera (2008) the W phase can be interpreted as superposition of the fundamental, first, second and third overtones of spheroidal modes or Rayleigh waves. Its group velocity varies between 4.5 and 9 km/s over a period range of 100 to 1000 s. The amplitudes of so long-period waves represent well the tsunami potential of great earthquakes. W phase inversion may yield reliable and non-saturating estimates of seismic moment and moment magnitude as well as of the source mechanism of large earthquakes within about 20 minutes of the earthquake occurrence (Fig. 2.75). Source inversion of the W phase has

recently been extended down to approximately Mw 6. Real-time implementations are operational at the U.S. Geological Survey's NEIC (Hayes et al., 2009) as well as at the GFZ Potsdam and the Indonesian Tsunami Early Warning System (InaTEWS).
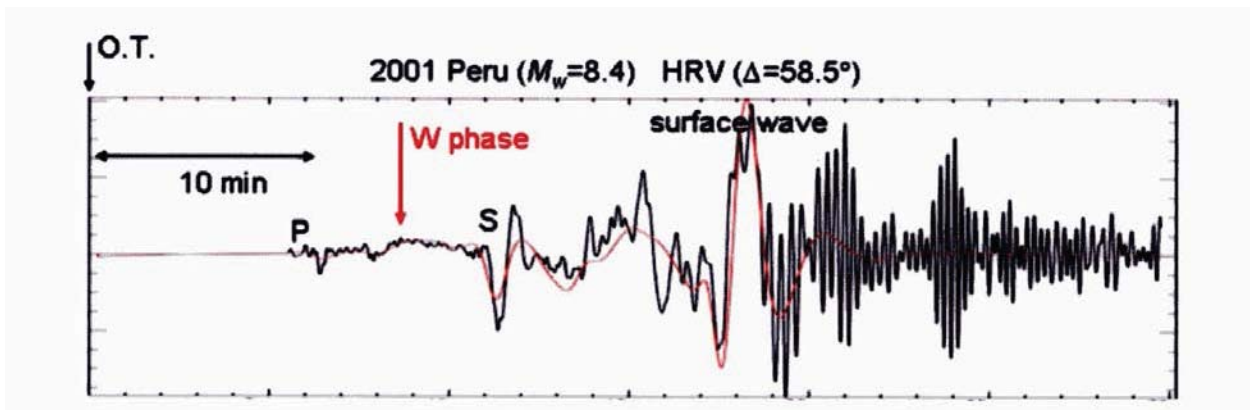

Fig. 2.74 W phase record of the 2001 Mw8.4 Peruvian earthquake at HRV superimposed with the synthetic W phase trace (red) computed by mode summation using the Global Centroid Moment Tensor solution for this earthquake (copy of Figure 1 on page 223 of Kanamori and Rivera, 2008; © Geophysical Journal International).
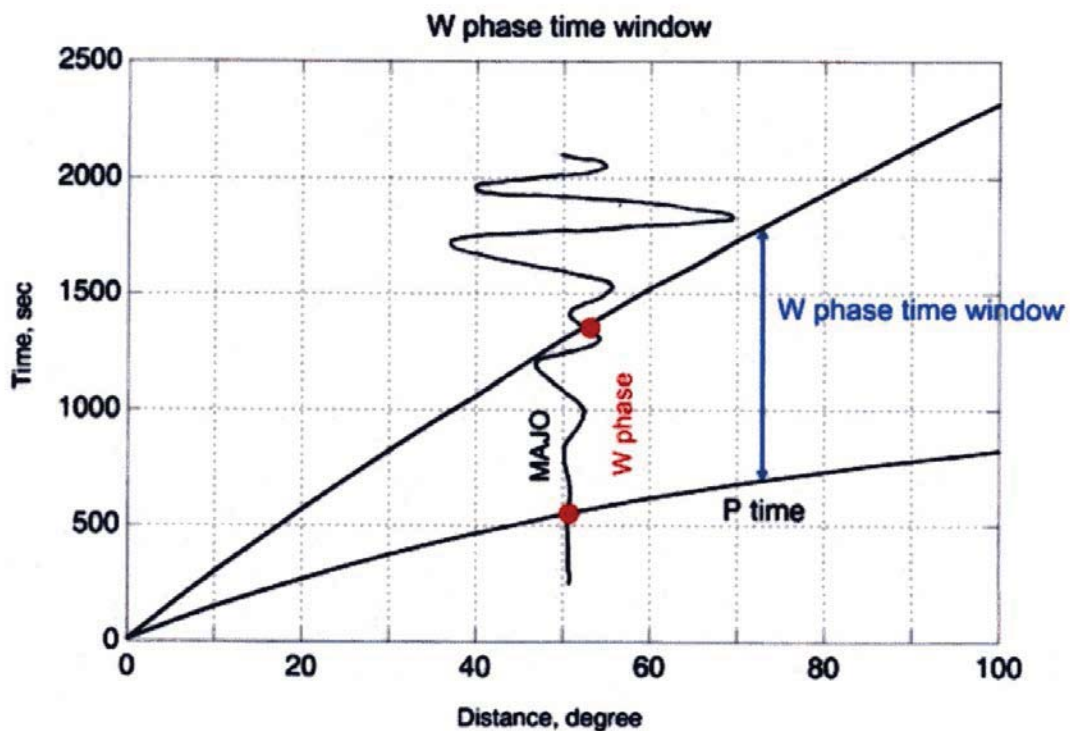

Fig. 2.75 Illustration of the distance-dependent time window within which W-phase observations are available for analysis after origin time. (Copy of Figure 15 on page 234 of Kanamori and Rivera, 2008; © Geophysical Journal International).